KSHV infects a subset of human tonsillar B cells, driving proliferation and plasmablast differentiation

Lynn M. Hassman,[1,2] Thomas J. Ellison,[1,2] and Dean H. Kedes[1,2,3]

[1]Myles H. Thaler Center for AIDS and Human Retrovirus Research, [2]Department of Microbiology, and [3]Department of Internal Medicine, University of Virginia Health Systems, Charlottesville, Virginia, USA.

Kaposi sarcoma–associated herpesvirus (KSHV; also known as HHV8) is the causative agent of two B cell tumors, multicentric Castleman disease (MCD) and primary effusion lymphoma (PEL). However, little is known about the nature of the specific B cell subtype(s) most susceptible to infection. Identifying these cells would provide direct insight into KSHV transmission and virus-induced transformation. To identify this subset and to determine whether infection alters its cellular phenotype, we exposed human tonsillar cells to KSHV and characterized infected cells using high-throughput multispectral imaging flow cytometry (MIFC). Stable expression of the virally encoded latency-associated nuclear antigen (LANA), a marker of latent KSHV infection, was observed predominantly in cells expressing the λ light chain of the B cell receptor. These LANA+ B cells proliferated and exhibited similarities to the cells characteristic of MCD (IgMλ-expressing plasmablasts), including blasting morphology with elevated expression of Ki67, variable expression of CD27, and high levels of IgM and IL-6 receptor. Furthermore, the proportion of infected cells showing a blasting phenotype increased upon addition of exogenous IL-6. Our data lead us to propose that oral transmission of KSHV involves the latent infection of a subset of tonsillar IgMλ-expressing B cells, which then proliferate as they acquire the plasmablast phenotype characteristic of MCD.

Introduction

Kaposi sarcoma–associated herpesvirus (KSHV/HHV8) is the causative agent of two B cell tumors, multicentric Castleman disease (MCD) and primary effusion lymphoma (PEL), as well as its namesake, Kaposi sarcoma. Both B cell tumors are fatal, and treatment to date prolongs survival by a few years at best (1, 2). MCD is a lymphoproliferative disorder, localized to the mantle zone of lymph nodes and the spleen, and comprising KSHV-infected plasmablasts expressing IgM exclusively with the λ light chain (3), as well as transcription factors that suggest the cells are at the plasmablast, or pre-plasma, cell stage of differentiation (4). Except in cases that have progressed to frank lymphoma, both the infected cells (3) and the virus (5) in MCD lesions are polyclonal, suggesting multiple infectious events and implicating infection, rather than transformation, as the driver of this disorder. The cytokine IL-6 also plays an important role in MCD. Murine models can recapitulate the clinical manifestations of MCD even in the absence of KSHV simply by dysregulating IL-6 (6, 7). Similarly, IL-6 receptor (IL-6R) blocking therapy can ameliorate MCD symptoms in some patients (8–10). While the majority of KSHV-infected B cells in MCD express IL-6R (3), the precise effects of IL-6 on KSHV-infected B cells remain unknown.

PEL is a highly malignant immunoblastic tumor that most frequently affects body cavities such as the pericardial or pleural spaces. This clonal B cell tumor has high intracellular levels of KSHV genomes, expresses the plasma cell surface marker CD138/syndecan 1 (11) with absent or very low levels of cytoplasmic Ig (reviewed in ref. 12). Like MCD, PEL expresses plasmablast stage-specific transcription factors (4).

Early investigations (13, 14) identified KSHV as the likely etiologic agent of these B cell tumors shortly after the virus's discovery in 1994 (15). Subsequent work detected KSHV DNA sequences specifically in the CD19+ (B cell) fraction of the peripheral blood of KSHV-infected patients (16, 17), and B cells from seronegative individuals were infectable ex vivo with KSHV isolated from a patient's tumor (17, 18). While many investigations have characterized the potential roles of KSHV gene products in B cell tumorigenesis using cell lines and single-gene studies, direct evidence that KSHV infection of human B cells leads to KSHV-associated tumors is lacking. Likewise, little to no data exist examining the nature of the B cells most vulnerable to initial infection.

Extensive molecular and seroepidemiologic data suggest that KSHV transmission occurs primarily via saliva (19, 20). In support of this, Chagas et al. found evidence of KSHV infection in approximately 10% of normal tonsils in Brazilian individuals (21). In situ hybridization experiments in that study revealed that infected cells were consistently present in the subepithelial region of the tonsil. The Chagas study did not identify the infected cells; however, the subepithelial region is heavily populated with IgM-expressing B cells that rapidly differentiate into proliferating antibody-secreting plasmablasts in response to oral pathogens (22, 23) and, therefore, represent a potentially favorable target for a latent virus that relies primarily on cellular replication for its propagation. At a minimum, the consistent presence of infected cells in one region suggested to us that KSHV might target a particular subset of tonsillar B cells.

B cells express either the κ or the λ Ig light chain, in addition to one of the heavy chain isotypes, IgM, IgG, IgA, or IgE. IgM is the first isotype naive B cells express, and expression of the other isotypes only occurs if the cells undergo Ig class switching. During B cell differentiation, cell surface Ig is downregulated as the cells begin to express and secrete Ig. Proliferative antibody-secreting cells are known as
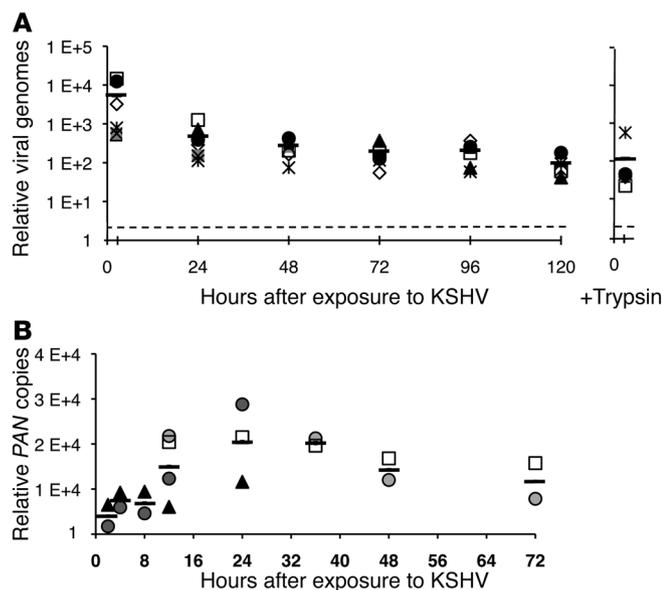
Figure 1

Levels of viral genome and *PAN* transcript associated with human tonsillar B cells following ex vivo inoculation with KSHV. Tonsillar B cells from 6 individual donors, represented by each symbol, were exposed to KSHV for 2 hours and washed extensively, and genomic DNA was purified at the indicated times. (**A**) Left panel: Relative levels of genomic KSHV DNA normalized to *GAPDH* for each time point were determined by qPCR and represent the approximate copies of ORF73/10e3 cells. Right panel: Relative levels of internalized viral genomes for all of the donors at 2.5 hpi determined as in the left panel but after first treating KSHV-exposed samples with trypsin to discriminate KSHV entry from surface binding. Values for each donor are mean of triplicate PCR reactions. Horizontal bars represent mean values for all donors at each time point. Dashed line represents mean level of background signal detected in 2.5-hour cultures unexposed to KSHV. (**B**) Levels of viral *PAN* RNA were similarly quantified and normalized to *GAPDH* using qRT-PCR from total RNA. Values represent the approximate number of *PAN* transcripts per 37.5 ng of input RNA. Open squares and filled triangles correspond to those in **A**; light and dark gray circles in **B** represent results of separate experiments on samples from the same tonsil donor. Horizontal bars represent mean values for all donors at each time point. Signal was below detection in no-RT reactions or uninfected samples (not shown).

plasmablasts. Some plasmablasts terminally differentiate into long-lived plasma cells, while others secrete antibody for a short time and then die. Terminal plasma cell differentiation is marked by surface expression of CD138 in the absence of most other B cell markers. PEL cells express CD138 and lack surface Ig, and are thus phenotypically more similar to plasma cells than the less-differentiated MCD B cells, which express both surface and cytoplasmic Ig and lack CD138 (4). Since B cell tumors likely represent normal B cells effectively stalled at a particular stage of differentiation by a transformative event(s) (24–26), the above Ig and CD138 expression profiles suggest that the transformation responsible for PEL may occur at a later stage of B cell differentiation than for MCD lymphomas.

Both tumors demonstrate that KSHV infection is present in B cells with either an early (MCD) or a late (PEL) plasmablast phenotype. While KSHV might specifically infect plasmablasts, thereafter stalling further differentiation, it is equally possible that it infects a less-differentiated cell and either initially leaves undisturbed the

normal differentiation program or, instead, actively drives the cell toward the plasmablast phenotype. Infection of a less-differentiated B cell would also suggest that PEL and MCD could potentially share a common progenitor, representing the subset of cells most susceptible to de novo KSHV infection, and that postinfection events might determine the final transformed phenotype.

We reasoned that if our hypothesis were correct, KSHV would initially infect a subset of tonsillar B cells that shared basic phenotypic characteristics with MCD, the less-differentiated tumor. At a minimum, these would include the original Ig isotype, IgM, as well as the λ light chain. To identify the cell type that potentially represents both the initial target of KSHV infection and the cell of origin for at least MCD and possibly PEL, we exposed primary human tonsillar B cells to purified KSHV and characterized the cells that became latently infected using multispectral imaging flow cytometry (MIFC), a high-throughput single-cell imaging technique.

Unlike traditional flow cytometry, MIFC quantifies localized signal intensities rather than merely total whole cell fluorescence. Previously, our laboratory showed that the number of detectable latency-associated nuclear antigen (LANA) dots per cell increases with MOI and correlates strongly, although not 1:1, with the number of viral genomes per cell (27), consistent with the well-characterized episomal tethering function of LANA protein aggregates (28–30). A limitation of previous MIFC experiments was the single-plane analysis performed with the earlier version of the software that could potentially underestimate the true number of LANA dots per cell. In the present study, we took advantage of improved optics and image-processing modifications that allow extended depth of field (EDF), generating confocal-like image projections with the entire cell simultaneously in focus (31). This allowed us an even more precise and sensitive detection of LANA dots within the nuclei of KSHV-infected human tonsillar B cells.

Results

Isolation of tonsillar B cells. We hypothesized that KSHV could establish latent infection in tonsillar B cells. To test this, we obtained deidentified tonsils from routine tonsillectomies and purified the B cell fraction by negative selection, thereby avoiding activation of surface receptors, which could potentially alter either KSHV tropism or target cell phenotype. Flow cytometry confirmed that the sorting procedure generated greater than 95% pure CD19+ B cells (data not shown). We then exposed the cells to fresh preparations of concentrated KSHV. In later experiments, to monitor potential infection of non-B cells as well as to assess potential differences in the pattern of B cell infection in a mixed culture, we omitted the physical B cell isolation step and infected tonsil mononuclear cells en masse. In this latter approach, we identified (and gated on) B cells within the cultures based on their expression of the Ig light chain κ or λ (see results below). We studied KSHV infection in tonsil cells from more than 50 donors in total, though the data in this study represent the outcome from 21 representative individuals.

Stable presence of viral genomes and pre-latent transcript expression in human tonsillar B cells following ex vivo inoculation with KSHV. To detect potential KSHV infection in human tonsillar B cells ex vivo, we exposed the cells to purified KSHV, washed the cells extensively to remove unbound virus, and quantified the amount of viral genomic DNA that remained associated with the cells over time. At early time points after exposure, we found a relatively high number of KSHV genomes associated with the B cells. This level

A
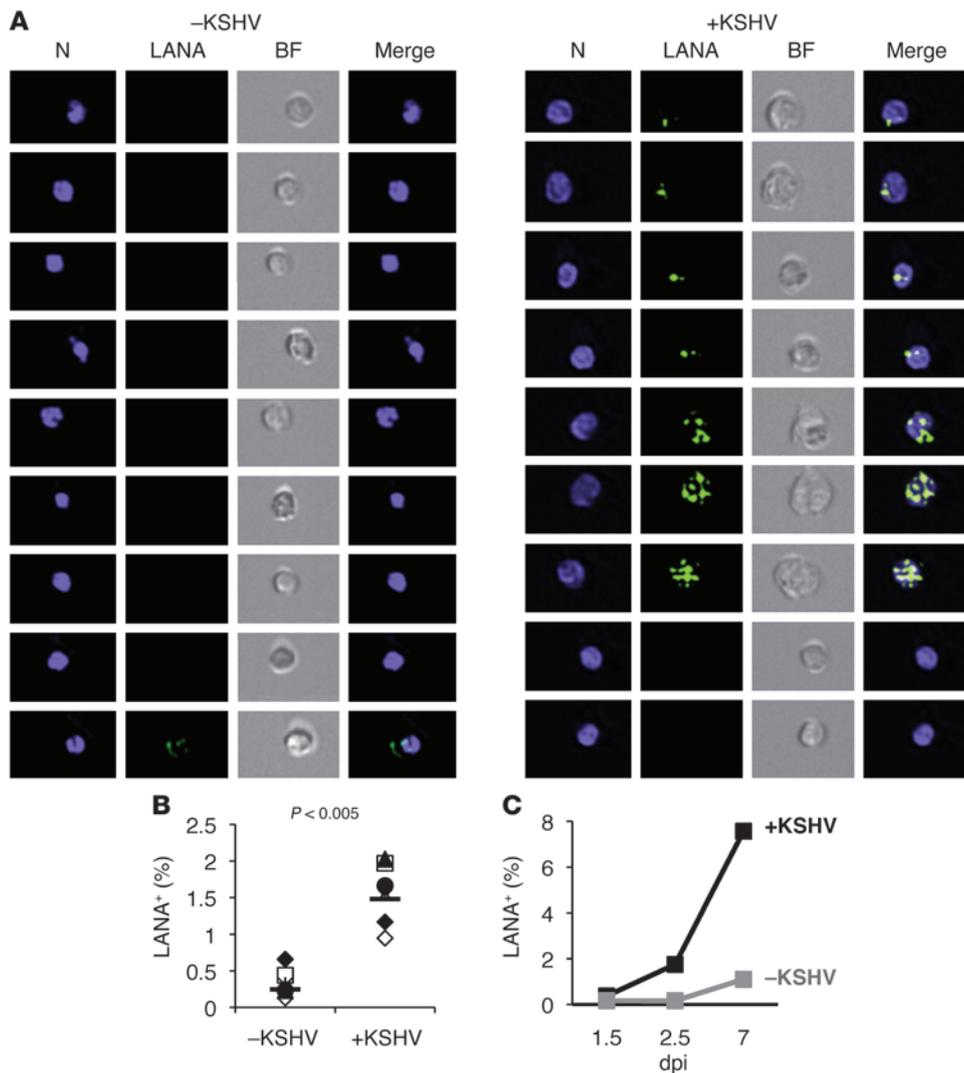
Figure 2
Expression and maintenance of LANA within human tonsillar B cells. MIFC was used to identify cells expressing characteristic nuclear LANA dots following KSHV infection of tonsillar B cells isolated from 6 donors. (**A**) Representative images of B cells from cultures unexposed (left panel) or exposed (right panel) to KSHV. (**B**) Isolated B cells were cultured in the absence or presence of KSHV, and the percentage of LANA dot–positive cells was determined at 60–84 hpi for individual donors represented by individual symbols. Horizontal bars represent the mean value for all donors. (**C**) Cells from a separate tonsil were cultured without (gray line) or with (black line) KSHV for the indicated times before MIFC analysis of B cells gated within the software. For analyses at 7 dpi only, cells were kept in the presence of CD40L-3T3 cells to maintain viability. N, DAPI-stained nucleus; BF, bright-field.

declined approximately 100-fold over 24–48 hours after infection (hpi) but then remained relatively stable for at least 5 days after infection (5 dpi) (Figure 1A).

We reasoned that the initially high levels of viral DNA may have represented bound but not internalized virus that eventually dissociated from the surface of the B cells. In support of this notion, we found that trypsinization at 2.5 hpi reduced the number of viral genomes by approximately 100-fold, similar to levels detected at 5 dpi without trypsinization (Figure 1A, compare right and left panels). This finding suggested that the viral DNA present at 5 dpi likely represented internalized KSHV genomic DNA, whereas the higher level of cell-associated virus at 2.5 hpi may have represented a transient binding of KSHV to the cell surface but not to actual entry receptors (32, 33). Consistent with this interpretation, we found that at 5 dpi, trypsin treatment of infected cells in a separate experiment had little effect on the levels of cell-associated KSHV DNA.

The persistence of a low number of KSHV genomes in the tonsillar B cell cultures was consistent with a latent, rather than lytic, infection. Although we could still detect low levels of infectious genomes in the supernatant 48 hpi, this likely represented residual virions from the initial inoculum, since inhibition of the viral polymerase by continuous treatment of the culture with 500 μM phos-

phonoacetic acid (PAA) (34) did not decrease these levels (data not shown). Furthermore, lytic replication of even a small fraction of the cells would have resulted in increasing levels of intracellular viral DNA. Instead, the levels were essentially unchanged between 2 and 5 dpi (Figure 1A). Taken together, these data suggested that the initial decrease in cell-associated virus between 2.5 hpi and 48 hpi and the small amount of virus in the media 48 hpi represented dissociation of cell-bound virus from the initial inoculum, rather than de novo lytic replication. The long-term persistence of trypsin-resistant viral DNA in tonsillar B cells, however, indicated that, at a minimum, KSHV gained entry into the cells.

To test whether internalized KSHV genomes were transcriptionally active in tonsillar B cells, we quantified the levels of the viral polyadenylated nuclear (*PAN/nut-1*) RNA by quantitative RT-PCR (qRT-PCR) amplification of total RNA. *PAN* RNA is a direct target of the KSHV transcriptional activator (RTA) and is highly abundant during lytic replication (35). Endothelial cells express *PAN* following de novo infection (36), as do tonsillar cells from asymptomatic KSHV-infected patients (21). In agreement with previous descriptions of this RNA as a component of the pre-latent (first termed "lytic burst") transcription program following de novo KSHV infection of primary endothelial cells (36), we detected *PAN* in tonsillar B cells beginning

at 2 hpi. The levels of *PAN* peaked at 24 hpi but trended downward thereafter (Figure 1B). Of note, we detected *PAN* in B cells from 14 of 14 tonsils that we assayed but found no evidence of this viral transcript in uninfected B cells or in no-RT control reactions.

On its own, *PAN* expression, and especially increasing levels of *PAN* expression, could be a bellwether for low levels of lytic replication. However, in light of (a) the transient nature of *PAN* expression in our culture system, (b) the stable, rather than increasing, intracellular viral DNA levels after infection (Figure 1A), and (c) the lack of the PAA effect on background levels of viral DNA in the supernatant (discussed above), our detection of *PAN* most likely reflected the transient burst of pre-latent genes that can occur after de novo infection (36).

Expression and maintenance of LANA within human tonsillar B cells. Because tonsillar B cells are a heterogeneous population comprising cells at various stages of cellular activation and differentiation, we hypothesized that infection would likely be unevenly distributed, potentially favoring a subset of susceptible cells that would be enriched for viral genomes. Furthermore, even among individual infected cells, we predicted that the number of viral genomes would vary stochastically, reflecting, at least initially, a Poisson distribution as we previously reported for de novo infection of other cell types (27).

To determine whether KSHV could establish latent infection in human tonsillar B cells, as well as to determine which fraction of cells were susceptible to infection, we incubated KSHV-exposed B cells with a monoclonal antibody directed against LANA. LANA forms a series of dimers or higher-order multimers that tether the viral genome to the host cell chromatin during latency (29, 37, 38). By immunofluorescence microscopy, episome-associated LANA appears as characteristic punctate nuclear dots, with increasing numbers of LANA dots correlating with increasing numbers of intracellular viral genomes (27). We predicted that KSHV-infected B cells might be rare in our cultures, so we employed MIFC, a highly sensitive and specific high-throughput imaging technique, to identify and characterize KSHV-infected (LANA-positive) cells (39). This approach combines the specificity of immunofluorescence microscopy with the statistical power of flow cytometry. To eliminate nonviable cells from our analyses (approximately 50% of tonsillar cells in our cultures die within 72 hours regardless of the presence of KSHV and in agreement with published findings; ref. 40), we treated the cells with DNase I (41) at the time of collection. We then confined our analysis to the cells that stained brightly for DAPI, which indicated that their cell membranes were impervious at the time of collection and had therefore excluded the DNase.

As we had predicted, MIFC analysis revealed that a small fraction of the total culture of tonsillar B cells expressed LANA in the characteristic punctate nuclear pattern 60–84 hours after exposure to KSHV (Figure 2A). We created an imaging algorithm within the MIFC analytical software to identify and enumerate cells that contained these nuclear LANA dots (see Methods). The percentage of tonsillar B cells that became LANA dot–positive following KSHV exposure varied by tonsil donor, ranging from 1% to 2%, but averaged approximately 1.5% (Figure 2B and additional results below). LANA dots were present in purified tonsillar B cells in a Poisson-like distribution as described previously (27), with a mean of 1.7 dots/cell. We did not detect LANA dots in cells that had not been exposed to KSHV (Figure 2A) or were exposed to UV-inactivated KSHV (data not shown).

While we routinely detected LANA dots in primary B cells between 48 and 96 hpi and were able to consistently detect viral genomes up to 5 dpi, we wanted to confirm the stability of KSHV infection by following the presence of LANA dots in these cells over longer periods. However, as primary human B cells in standard lymphocyte media survive for only limited times in culture, we utilized a feeder layer of CD40L-expressing 3T3 fibroblast cells (CD40L-3T3 cells) to provide survival signals (42) to our longer-term cultures. This system allowed us to follow KSHV-exposed tonsillar B cells for 1–2 weeks with a viability (trypan blue and DNase exclusion) of approximately 45%.

To assess whether the fraction of infected B cells was stable over time, we infected tonsil cells en masse and followed the B cells (identified by expression of Ig light chain) longitudinally for the presence of LANA. Figure 2C shows an example of such an experiment; LANA was not evident at 1.5 dpi, but rose to approximately 2% by 2.5 dpi. Furthermore, in a sister culture grown in the presence of CD40L-3T3 support cells, the B cells remained alive and infected for at least 1 week, and the fraction of LANA+ cells continued to increase. Figure 2C shows, with this specific tonsil, that the percentage of LANA+ cells rose to approximately 8% by 7 dpi. Although we did not definitively determine whether the increased level of infection within the culture at later time points was due to the enhanced survival or proliferation of infected cells or to infection of new targets, we did not detect significant lytic virion production in our system (discussed above), while we did document KSHV-driven proliferation (see below). We utilized the CD40L-3T3 feeder layer for this experiment as a means of maintaining cell viability while determining whether LANA dot–positive cells persisted at longer time points after infection. The results indicated that infection remained in the primary human tonsillar B cells for up to 2 weeks after infection.

We also found that long-term culture and/or the feeder cell coculture led to a slightly higher background LANA signal, with the automated software detecting nonspecific dots at 7 dpi more frequently than at 72 hpi (Figure 2C). Individual images of cells with aberrant LANA signal in the older cultures unexposed to KSHV appeared consistent with the nonspecific, usually atypical single-dot pattern found in unexposed cultures at 72 hpi (see Figure 2A, left, bottom row, for an example). This pattern of fluorescence may represent either nonspecific labeling with the monoclonal anti-LANA antibody or autofluorescence that is evident in older cultures in the same fluorescence channel as the Alexa Fluor 488–conjugated anti-LANA antibody. In marked contrast, the vast majority of the LANA+ cells in the KSHV-exposed cultures at all time points demonstrated a characteristic intranuclear punctate pattern, with many showing numerous distinct dots (compare background staining at 72 hpi in Figure 2A, bottom row on the left, with true LANA+ cells on the right). Within the confines of the time points we examined, these data indicate that KSHV can establish a latent-appearing (LANA+) infection in a small fraction of human tonsillar B cells.

KSHV targets λ B cells for stable LANA+ infection. We consistently detected LANA dots in only a small fraction of the tonsillar B cells, supporting our hypothesis that latent (LANA+) KSHV infection may be restricted to a subset of B cells. We further hypothesized, however, that this subset may resemble the KSHV-infected cells found in the KSHV-associated B cell tumor, MCD. MCD plasmablasts express exclusively the λ light chain of the B cell receptor, a phenotype that is fixed at the B cell precursor stage (43). We hypothesized that the normal counterpart(s) of, or initial precursor to, KSHV tumor cells may also share this Ig light chain bias.
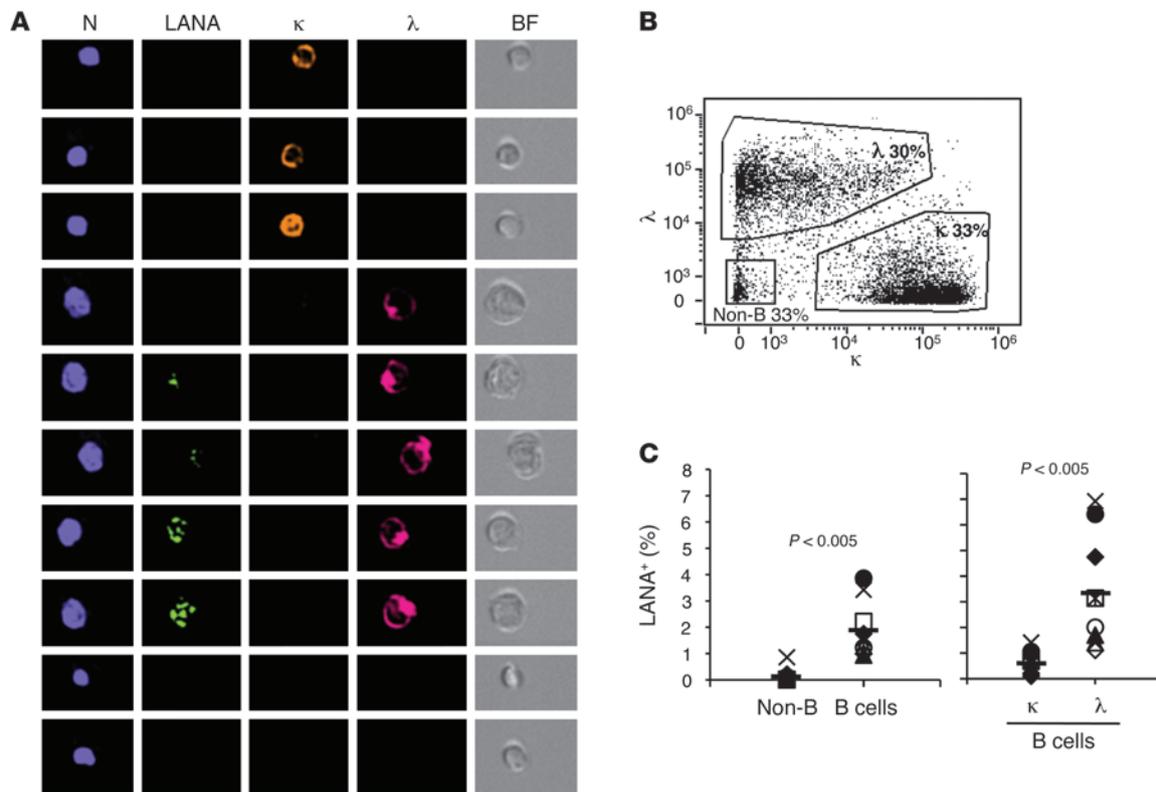
Figure 3
LANA expression is evident primarily in λ tonsillar B cells. Tonsil cells from 8 donors were exposed to KSHV and analyzed by MIFC at 60–84 hpi to determine susceptible subsets. (**A**) Representative images of cells labeled with antibodies to LANA, κ, and λ. (**B**) Representative scatter plot of κ versus λ staining of tonsillar cells. Gates were drawn to include all B cells (λ+ + κ+) versus non-B cells (λ– κ–). (**C**) Left panel: Percentage of non-B cells (λ– κ–) or B cells (λ+ + κ+) expressing LANA dots from individual donors represented by individual symbols. Right panel: Percentage of κ or λ B cells expressing LANA dots from individual donors represented by symbols that correspond to those in the left panel. Horizontal bars represent the mean value for all donors.

To identify the target B cell subset(s) as well as any potential non-B cell targets of LANA+ KSHV infection ex vivo, we exposed unpurified tonsil cell suspensions to KSHV and labeled these cells with antibodies directed against the Ig light chains κ and λ in addition to the viral protein LANA (Figure 3A) at 60–84 hpi. Consistent with earlier descriptions of tonsillar composition, we found that the tonsils we examined contained approximately 50%–70% B cells, 30%–50% T cells, and a small percentage of monocytes/dendritic cells (44, 45) both before KSHV exposure and 72 hpi (data not shown). Since expression of either κ or λ defines all B cells, and absence of both markers defines non-B cells, we employed this simple algorithm to define these two populations. Using MIFC analytical software, we gated the KSHV-exposed tonsil cells into non-B and B cells (30%–45% and 50%–65% of viable cells, respectively) (see Figure 3B for representative gating) and then assessed for the presence of LANA dots in each of the two populations. In all of our analyses, we similarly assessed for LANA+ cells in control cultures that were not exposed to KSHV to confirm the specificity of anti-LANA staining. Figure 3C, left panel, shows that LANA+ cells were evident exclusively in the B cell fraction and not in the non-B cells (comprising almost entirely T cells) in agreement with the detection of viral genomes predominantly in the CD19+ (B cell) fraction of peripheral blood cells from seropositive patients (16). Thus, LANA+ KSHV infection preferentially occurred in B cells within ex vivo suspensions of human tonsil-

lar cells. Of note, in separate experiments, we also directly compared the rates of KSHV infection in purified B cell cultures with cultures from the same tonsil donor (n = 5) that contained non-B cells (mixed cultures) and found no consistent effect on the overall percentage of KSHV-infected B cells (data not shown).

After subdividing the B cells by their expression of either κ or λ light chain, we found that LANA+ cells were overwhelmingly evident in the λ rather than the κ subset (Figure 3C), even though each subset was present in the tonsillar cultures in nearly equal proportions (Figure 3B). The preference for λ over κ was marked, with the latter demonstrating levels and patterns of LANA signal that were barely distinguishable from the background staining evident in uninfected controls. The strong λ B cell preference was evident regardless of the presence or absence of non-B cells in cultures and persisted in cells from two tonsil donors, even at 7–14 dpi within cells cocultured on the CD40L feeder layer.

In contrast to the clear predilection for LANA expression in λ B cells, we have detected *PAN* RNA in κ B cells and CD3+ T cells as well as in λ B cells, sorted 24 hours after en masse infection of tonsil cell suspensions (our unpublished observations). The presence of this transcript in a broader range of cell types would suggest that, at least under the conditions of our ex vivo infection system, viral entry and pre-latent gene transcription were less discriminatory than LANA expression.
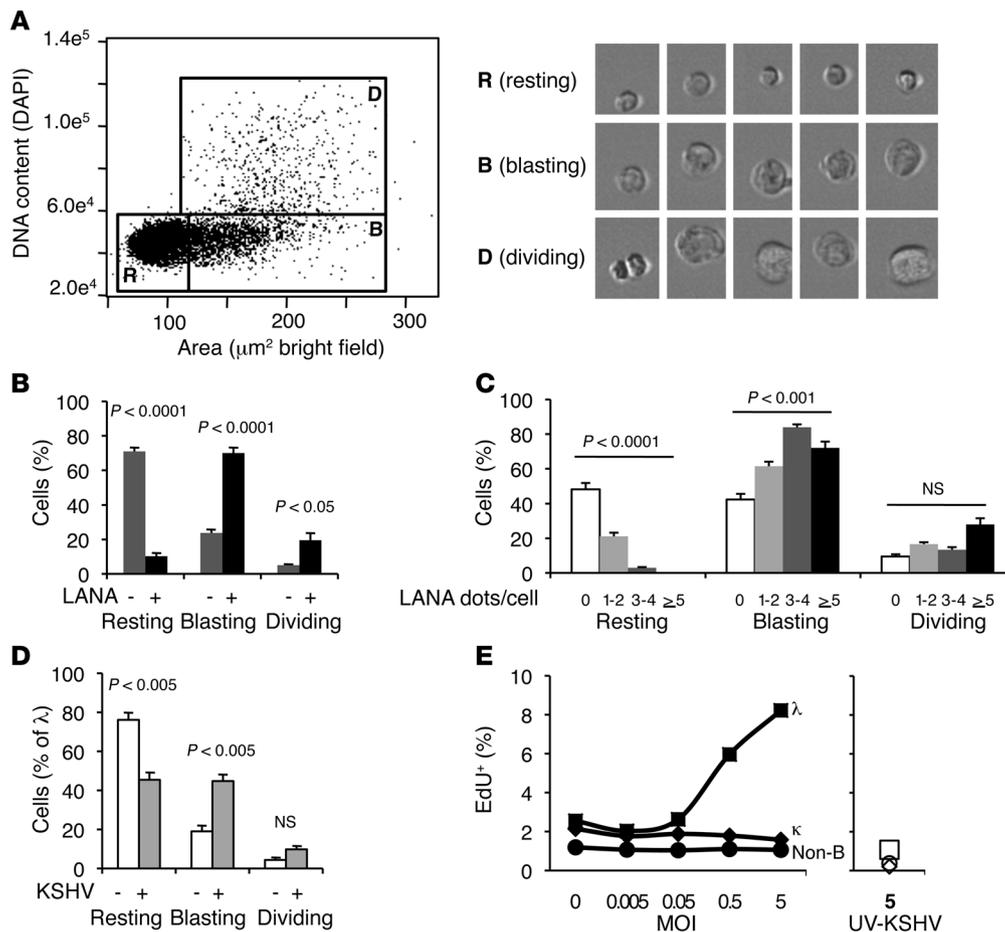
Figure 4

Growth and proliferative effects of KSHV on latently infected B cells. Tonsil cell suspensions were exposed to KSHV and analyzed for growth and proliferation by assessment of the area (of bright-field image) and DNA content (intensity of DAPI staining) of individual cells, respectively, at 48–84 hpi. (**A**) Representative scatter plot of area by DNA content (left), and images of representative cells from each gate (right). Three populations were evident, differing in size and/or DNA content: small (<110 μm^2, gate R, resting), large (>110 μm^2, gate B, blasting), and large with increased DNA content (gate D, dividing). (**B**) Distribution of these 3 cell types within LANA$^-$ (gray bars) and LANA$^+$ (black bars) cells in cultures exposed to KSHV. Data represent mean ± SEM of 7 tonsil donors. (**C**) LANA$^+$ cells were gated according to their intracellular viral load, with groups containing 1–2 (light gray), 3–4 (dark gray), or ≥5 (black) LANA dots/cell. Percentages of resting, blasting, and dividing cells were determined for 7 tonsil donors. P values refer to Spearman correlations, which were −0.937 for resting, 0.619 for blasting, and 0.37 for dividing. (**D**) Distribution of resting, blasting, and dividing cells within λ B cells unexposed (white bars) or exposed (gray bars) to KSHV for 7 tonsil donors. (**E**) Percentage of λ (squares), κ (diamonds), and non-B (circles) cells that incorporated the nucleoside EdU following exposure to increasing MOI of KSHV (left) or UV-inactivated KSHV (right). Results shown are representative of 3 different experiments.

KSHV-driven growth/proliferation in tonsillar B cells. We observed that the LANA$^+$ cells appeared larger than LANA$^-$ cells and hypothesized that KSHV infection may drive growth and/or proliferation of tonsillar B cells. To address this possibility, we compared the cell size (area of the bright-field image) and DNA content (intensity of DNA staining with DAPI) in our cultures at 48–84 hpi. The left panel of Figure 4A shows a representative scatter plot, with each pixel representing an individual cell, in which we identified and gated cells that were small (<110 μm^2) with low DNA content, designating them as resting (R); large (>110 μm^2) with low DNA content, designating them as blasting (B); and large with increased DNA content, designating them as dividing (D). The right panel of Figure 4A depicts representative images from each of these gates, R, B and D. The images show that some cells in the D gate do, in fact, appear to be undergoing early stages of cytokinesis. We then characterized the extent of proliferation of LANA$^-$

and LANA$^+$ cells by comparing their distribution within each of the above gates. LANA$^-$ cells were predominantly resting (75%), whereas only 10% of LANA$^+$ were resting. Only about 20% of LANA$^-$ cells were blasting, in contrast to the majority (70%) of LANA$^+$ cells. Finally, a small fraction (5%) of LANA$^-$ cells were dividing, while a significantly greater portion (20%) of LANA$^+$ cells were dividing (Figure 4B).

To address more rigorously the link between KSHV infection and promotion of cellular growth, we subdivided LANA$^+$ cells by intracellular viral load, gating them into groups with 1–2, 3–4, or ≥5 LANA dots/cell. We then assessed each group for the percentage of cells that were resting, blasting, or dividing. We found that intracellular viral load positively correlated with the fraction of proliferating cells. The cells with the lowest viral load (0 or 1–2 LANA dots/cell) had the highest fraction of resting cells, while the group with the highest viral load (≥5 LANA dots/cell) had the low-
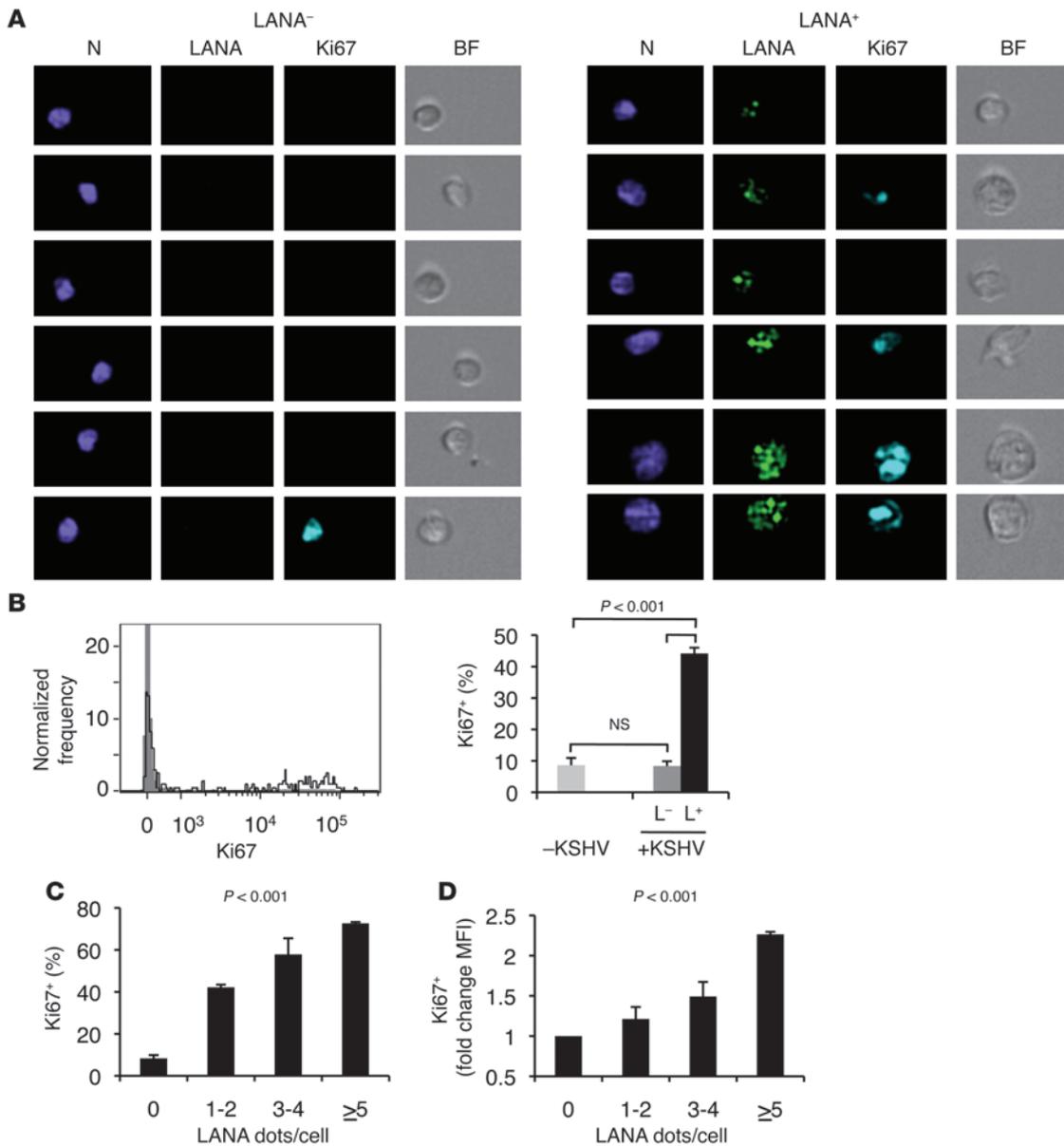
Figure 5
KSHV-induced expression of the proliferation marker Ki67. Tonsil cells were analyzed for the expression of LANA and the proliferative marker Ki67 72 hpi using MIFC. (**A**) Representative images of LANA⁻ and LANA⁺ cells labeled with antibodies directed against LANA and Ki67 following KSHV exposure. (**B**) Left panel: Histogram showing Ki67 expression in LANA⁻ (gray filled) and LANA⁺ (black line) cells. Right panel: Mean percentage (±SEM) of cells expressing Ki67 unexposed to KSHV (light gray bar); exposed to KSHV but LANA⁻ (gray bar); or exposed to KSHV and or LANA⁺ (black bar). (**C**) Mean percentage (±SEM) of cells expressing Ki67 gated according to relative intracellular viral load into groups with 0, 1–2, 3–4, or ≥5 LANA dots/cell. *P* value refers to Spearman correlation, which was 0.902. (**D**) Mean (±SEM) fold change in levels of Ki67 expression was assessed by dividing the Ki67 MFI of each of LANA⁺ group (gated as in **C**) by the Ki67 MFI of LANA⁻ cells. Only Ki67⁺ cells were analyzed. Data represent mean ± SEM from 4 separate tonsil donors. *P* value refers to Spearman correlation, which was 0.792.

est (Figure 4C). Significantly, all of the cells with highest viral load, and nearly all of the cells with intermediate viral load were either blasting or dividing. This positive correlation suggested either that KSHV infection drove B cell proliferation or that KSHV more efficiently infected proliferating cells.

To help distinguish between these two possibilities, we compared the proportion of proliferating cells among each subpopulation of tonsillar cells in the presence or absence of KSHV. We reasoned that

if KSHV drove cells toward a proliferative state, rather than merely targeting proliferating cells extant in the culture prior to viral exposure, we would find a greater fraction of proliferative cells in the KSHV-exposed cultures than in the unexposed cultures. The results demonstrated that while the distribution of resting, blasting, and dividing cells within both non-B cells and κ B cells was unaffected by the presence of KSHV (data not shown), the proportion of proliferating λ B cells increased markedly with KSHV exposure (Figure 4D).

In the absence of KSHV, approximately 75% of λ B cells were resting, whereas in the presence of KSHV, this fraction was reduced to 45%, while the fraction of blasting cells more than doubled from 19% (–KSHV) to 45% (+KSHV). Likewise, the fraction of dividing cells significantly increased in the presence of KSHV from 4% (–KSHV) to 10% (+KSHV). These findings indicated that KSHV infection specifically drove proliferation of λ B cells.

Notably, the proportion of proliferating cells following KSHV exposure was greater than the proportion that became detectably LANA+. This suggested that KSHV infection resulted in a bystander effect on other λ B cells. Alternatively, although perhaps less likely, the apparently LANA– portion of the proliferating λ B cells could be infected but be at an early stage prior to well-organized LANA tethering of the episome(s) to the chromatin. The MIFC algorithm queried punctate LANA dots and thus would not detect cells with LANA expressed at a low level or broadly distributed (46).

To confirm that λ B cells proliferated after KSHV infection as suggested by their morphological changes and increased DNA staining (above), we also measured DNA synthesis. We exposed tonsil cultures to increasing amounts of KSHV or, as a negative control, UV-inactivated KSHV, and quantified the number of cells that incorporated the nucleoside analog EdU from 12 hpi to 72 hpi. We observed a clear positive correlation between the proportion of EdU+ λ B cells and the initial MOI. This correlation was absent for both κ B and non-B cells (Figure 4E). The percentage of λ B cells undergoing DNA synthesis, therefore, increased with infectious dose, again arguing that KSHV infection drove proliferation of λ tonsillar B cells. We also found that UV-inactivated KSHV had no effect on proliferation of any of the tonsillar cells, including the λ cells (Figure 4E, right panel), suggesting that proliferation required establishment of infection rather than mere viral binding to or entry into the cell.

To further investigate KSHV-driven proliferation in B cells, we assessed expression of Ki67, a nuclear antigen expressed during all stages of the cell cycle except G_0 (47) at 72 hpi. Figure 5A shows representative images of LANA– (left) and LANA+ (right) cells exposed to KSHV. A total of 8% of KSHV-naive cells expressed Ki67. Similarly, 8% of KSHV-exposed but uninfected (LANA–) cells expressed this marker, indicating that there was no bystander effect of KSHV infection on Ki67 expression in LANA– cells. In contrast, 44% of KSHV-exposed, LANA+ cells were Ki67+ (Figure 5B). These results corroborated the marked increases we found in cell size, DNA content, and EdU incorporation associated with KSHV infection.

We further explored the relationship between KSHV infection and proliferation by grouping LANA+ cells by viral load into cells with 1–2, 3–4, and >5 LANA dots/cell and measured the levels of Ki67. The proportion of infected cells expressing Ki67 rose with increasing intracellular viral loads, reaching nearly 75% for cells with 5 or more LANA dots (Figure 5C). We next asked whether KSHV infection also increased Ki67 expression on a per-cell basis as a function of viral load. To do this, we calculated the fold increases in Ki67 MFI in LANA+ cells compared with LANA– cells. Again, we found that the Ki67 expression levels correlated with increasing viral load (Figure 5D), increasing from a baseline set at 1 (0 LANA dots/cell) to 1.2-, 1.5-, and 2.3-fold for cells with 1–2, 2–3, and >5 LANA dots/cell, respectively. We also noted that the maximum Ki67 signal in LANA+ cells exceeded the maxima in KSHV-unexposed cultures. This dose-dependent relationship between viral load and Ki67 expression again suggested that latent (LANA+) KSHV infection was the driving force underlying the proliferation of infected λ B cells we observed.

Evidence of plasmablast differentiation in KSHV-infected λ B cells. It was of interest to us that the establishment of latent (LANA+) KSHV infection only within λ B cells was reminiscent of a similar, nearly exclusive λ bias evident in KSHV+ MCD and in at least some KSHV+/EBV– PEL B cell tumors (4). Since MCD is less differentiated and less neoplastic than PEL and, thus, potentially more similar to newly infected, nontransformed B cells, we focused our phenotypic analyses on a comparison between de novo infected tonsillar B cells and MCD plasmablast B cells. Specifically, we assessed LANA+ cells for the expression of surface markers expressed on MCD B cells, namely IgM, CD27, and IL-6R, as well as morphologic characteristics suggestive of the plasmablast stage of B cell differentiation, including cell size and the pattern of Ig expression.

To determine whether de novo infection of tonsillar B cells preferentially occurred within the IgM+ subset, we incubated KSHV-exposed tonsillar cells with antibodies directed against this marker (representative images shown in Figure 6A) at 72 hpi. We gated tonsillar cells into IgM+ and IgM– subsets (representative gating shown in Figure 6B, left panel) and assessed these fractions for the presence of LANA+ cells, as we described above for λ and κ B cells as well as non-B cells. Nearly all the LANA+ cells were present in the IgM+ subset while being virtually undetectable in the IgM– subset (comprising both IgM– B cells and non-B cells, Figure 6B, right panel), similar to the λ bias. This observation narrowed the identity of B cells targeted by KSHV for latent (LANA+) infection to the IgMλ subset.

Furthermore, within the IgM+ subset, the level of IgM expression on LANA+ cells was greater than on LANA– cells (Figure 6C, left panel, shows a representative histogram) and the fold change in intensity of IgM staining over that of LANA– cells increased with increasing viral load (Figure 6C, right panel). Together, these findings suggested that in addition to selectively establishing infection in IgM+ B cells, KSHV upregulated IgM expression.

Since we permeabilized the cells before staining, we measured total Ig expression, both surface and cytoplasmic. Examination of individual images revealed two distinct staining patterns that generally segregated with the absence or presence of LANA staining. The LANA– and LANA+ cells displayed a pattern suggestive of surface (Figure 6A, left panel) and surface plus cytoplasmic (Figure 6A, right panel) IgM expression, respectively. The apparent presence of surface IgM on LANA+ cells (as well as λ, Figure 3A) suggested that they were less differentiated than plasma cells and PEL cells, both of which lack surface Ig (12). However, LANA+ B cells appeared to additionally contain some cytoplasmic Ig (Figure 3A and Figure 6A, right panel) similar to MCD B cells (4), suggesting that the de novo infected, LANA+ B cells were likely in an early plasmablast differentiation state at 72 hpi.

We next compared the proportion of cells expressing CD27 in LANA+ versus LANA– cells, restricting our analysis to IgM+ B cells, thereby excluding CD27+ tonsillar T cells also present in the cultures. Figure 6D, left panel, shows a representative histogram illustrating the CD27+ gate as well as the comparison of CD27 expression on LANA– and LANA+ IgM+ cells. Overall, CD27 expression was low (relative to T cells) on tonsillar B cells; however, since MIFC allows visual inspection of CD27 expression in each region of the histogram, we were able to determine a threshold gate to distinguish between cells with and without discernible CD27 staining (Figure 6D, above left). Figure 6D, right panel, shows that among the IgM+ cells, the latently infected (LANA+) cells were enriched 4.5- to 30-fold (depending on the individual donor) for CD27 expression at 72 hpi compared
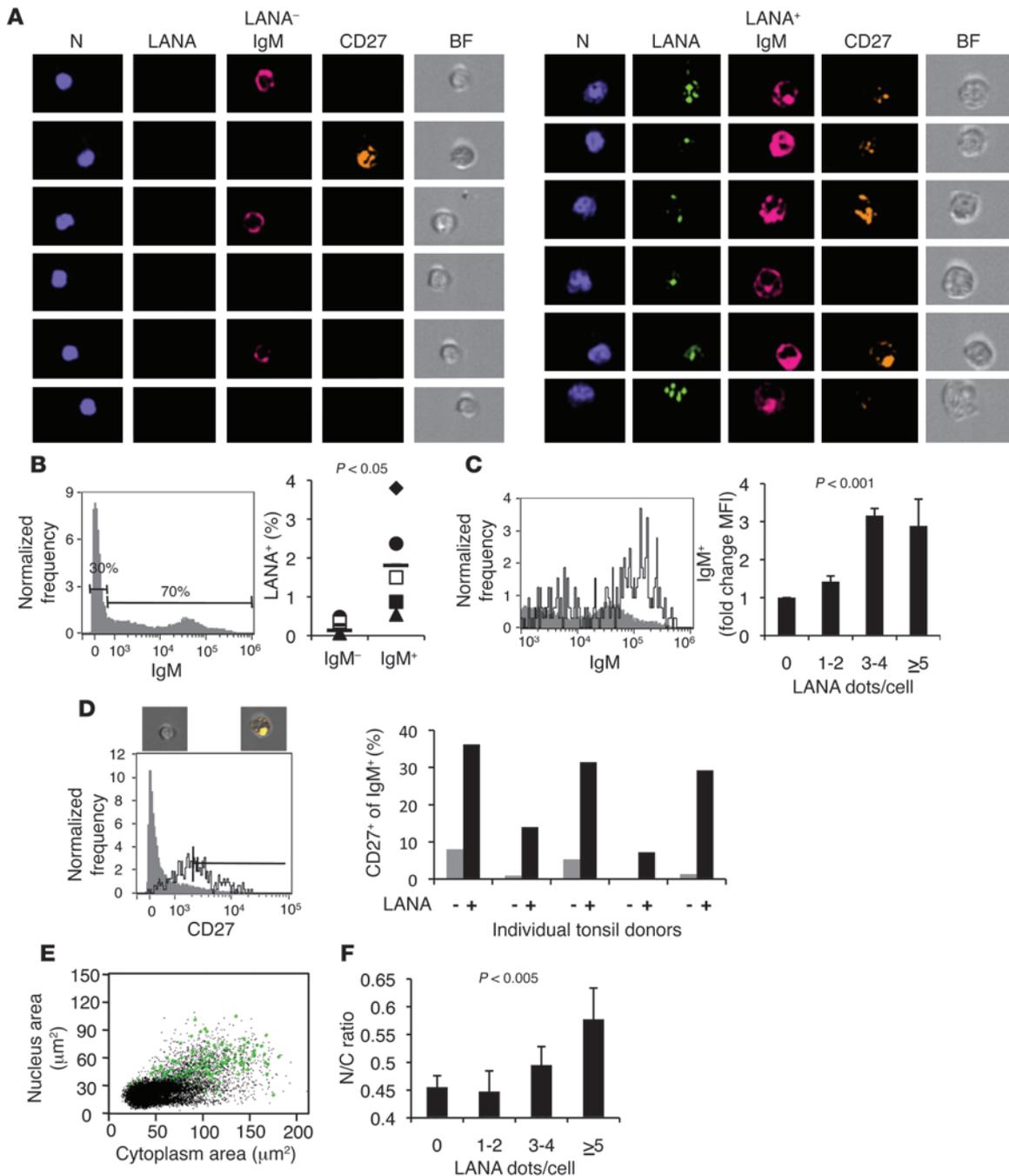
Figure 6
KSHV-infected B cells resemble MCD plasmablasts. Tonsil cells were exposed to KSHV and analyzed by MIFC for expression of LANA, IgM, and CD27 at 72 hpi. (**A**) Representative images of cells labeled with antibodies to LANA, IgM, and CD27. (**B**) Left panel: Histogram showing representative gating for IgM+ cells. Right panel: Percentage of IgM− or IgM+ cells expressing LANA dots, from 5 donors (individual symbols). (**C**) Left panel: Histogram showing, among IgM+ cells (gated as in **B**), levels of IgM expression on LANA− (gray line) versus LANA+ (black line) cells. Right panel: Among IgM+ cells, fold change in IgM expression (MFI) of individual LANA+ groups (1–2, 3–4, ≥5 dots/cell) compared with LANA− (0 dots) cells. Values represent mean ± SEM from 5 separate tonsil donors. *P* value reflects significance of Spearman correlation, which was 0.797. (**D**) Left panel: Representative histogram showing CD27 expression on LANA−IgM+ (gray filled) and LANA+IgM+ (black line) cells. Vertical line indicates threshold above which CD27 signal becomes visible by MIFC. Above left: Examples of cells on either side of threshold. Right panel: Percentage of IgM+LANA− or IgM+LANA+ cells expressing CD27 (5 donors). (**E**) Scatter plot showing nuclear and cytoplasmic areas for LANA− cells (gray dots) and LANA+ cells (green circles). (**F**) Mean N/C ratios for uninfected (0 dots) and cells with low (1–2 dots), moderate (3–4 dots), and high (≥5 dots/cell) viral load. Data represent mean ± SEM from 4 of 6 KSHV-exposed tonsils. *P* value reflects significance of Spearman correlation, which was 0.675.
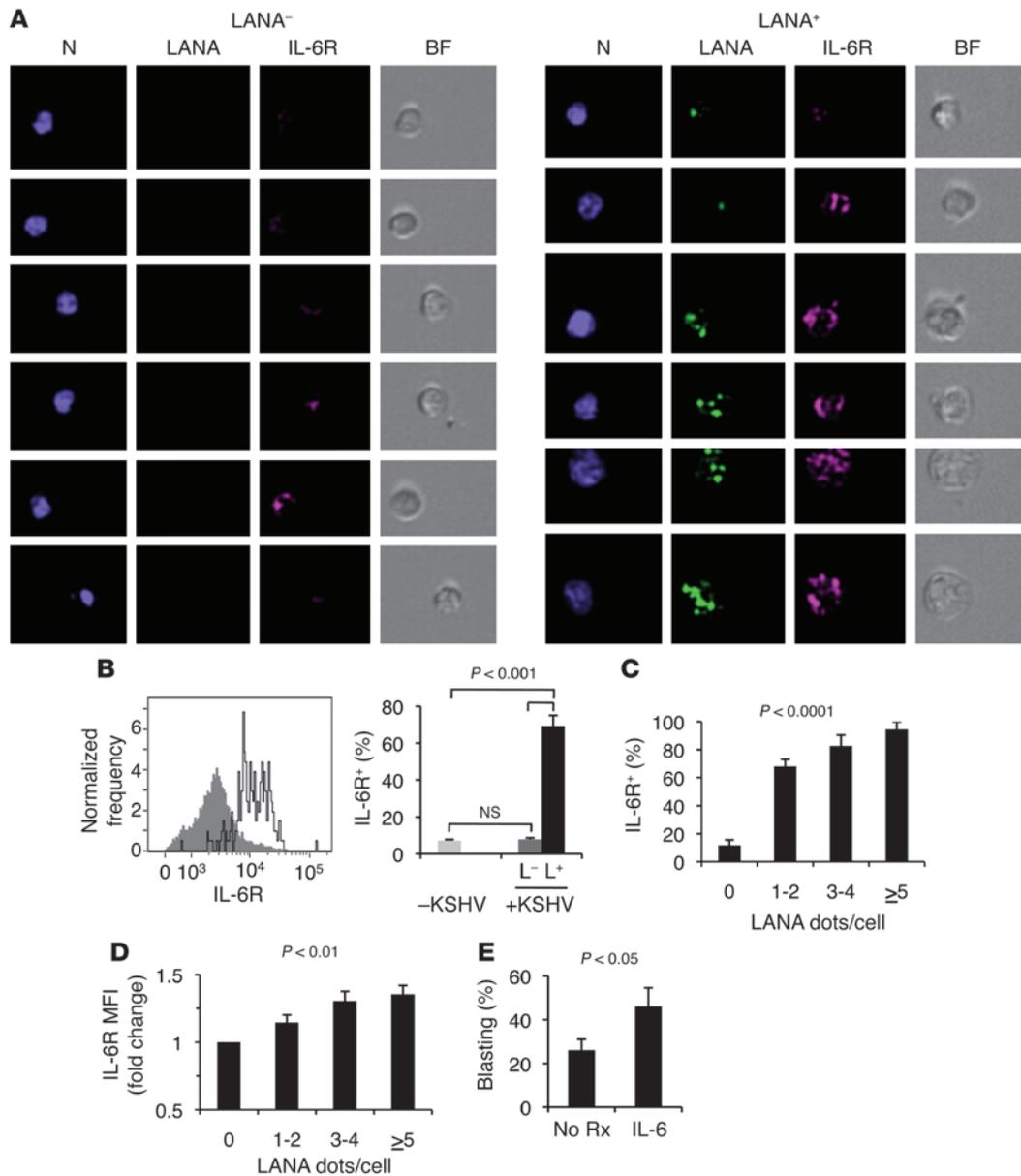
Figure 7
KSHV-infected B cells express high levels of IL-6R and respond to the plasmablast growth factor IL-6. (**A**) Representative images of cells labeled with antibodies directed against LANA and IL-6R at 72 hpi (LANA⁻ cells, left panel; LANA⁺ cells, right panel). (**B**) Left panel: Representative histogram showing IL-6R expression, gating for LANA⁻ (gray filled) and LANA⁺ (black line) cells. Right panel: Mean percentage (±SEM) of cells expressing IL-6R in cultures not exposed to KSHV (light gray bar) or exposed to KSHV and either LANA⁻ (dark gray bar) or LANA⁺ (black bar). (**C**) Mean percentage (±SEM) of IL-6R⁺ cells as a function of LANA dots/cell for 4 tonsil donors. *P* value refers to Spearman correlation, which was 0.878. (**D**) Mean (±SEM) fold change in levels of IL-6R expression was assessed by dividing the IL-6R MFI of individual LANA⁺ groups by the IL-6R MFI of LANA⁻ cells. Only IL-6R⁺ cells were analyzed. Data represent mean ± SEM from 4 separate tonsil donors. *P* value refers to Spearman correlation, which was 0.686. (**E**) Mean (±SEM) fold change in percentage of blasting cells within LANA⁺ population following exogenous IL-6 treatment (40 ng/ml) of cells from 4 individual donors.

with uninfected (LANA⁻) B cells. In contrast to our findings with Ki67 and IgM, both the level and likelihood of CD27 expression were approximately the same regardless of the number of LANA dots/cell, indicating that CD27 expression did not correlate with intracellular viral load. Of note however, between 7% and 36% of LANA⁺ cells were CD27⁺, a finding that mirrors the phenotype of KSHV-infected B cells in MCD (48).

In addition to the overall increase in cell size (Figure 4A and Figure 6E), we noticed that the nuclei of LANA⁺ cells were larger (Figure 6E). A hallmark of both normal and MCD plasmablasts is increased nuclear-to-cytoplasmic (N/C) ratio. To assess the N/C ratio of the ex vivo infected tonsillar B cells, we created MIFC software algorithms to calculate the ratio of the area of the DAPI-stained nucleus to the area of the bright field–defined cytoplasm (see Methods). We noted

inter-tonsillar variability in the N/C ratio among the 6 tonsils we examined, even though each demonstrated an overall increase in both nuclear and cytoplasmic areas. In 2 of the tonsils, the N/C ratio was essentially unchanged by the presence or absence of LANA dots. In the remaining 4 tonsils, however, we observed a positive correlation between the N/C ratio and intracellular viral load. LANA⁻ cells and LANA⁺ cells with the lowest viral load (1–2 LANA dots/cell) had similar N/C ratios, whereas cells with intermediate and higher viral loads (3–4 and >5 LANA dots/cell) had N/C ratios that were at least 10% and 30% higher, respectively (Figure 6F). This positive correlation suggested that, at least for these tonsils, KSHV induced this phenotypic change. In summary, de novo infected B cells shared phenotypic similarities with MCD plasmablasts, including proliferation and expression of Ki67, high levels of IgM, intermediate levels of CD27, and, in most cases, an increased N/C ratio.

KSHV-driven plasmablasts are responsive to IL-6. Given the central role of IL-6 in KSHV-associated disease (49, 50) as well as in normal plasmablast growth (51), we asked whether KSHV-infected tonsillar B cells were capable of responding to this cytokine. We first assessed the expression of IL-6R, a characteristic marker of both normal and MCD plasmablasts (3, 51), by MIFC at 72 hpi. Figure 7A shows representative images of IL-6R staining on LANA⁻ (left) and LANA⁺ (right) cells. The left panel of Figure 7B depicts a representative histogram of IL-6R expression on LANA⁻ and LANA⁺ cells from one tonsil donor. Quantitative characterization of cells from each (4) tonsil donor consistently revealed that the percentage of cells expressing IL-6R was similarly low on uninfected (LANA⁻) cells, whether KSHV-unexposed (7.1%) or -exposed (7.9%), whereas LANA⁺ cells were significantly enriched for IL-6R expression (69%) (Figure 7B). Moreover, the proportion of cells demonstrating detectable IL-6R expression correlated positively with viral load (Figure 7C). Furthermore, the level of expression on individual IL-6R⁺ cells similarly paralleled viral load. Figure 7D shows a positive correlation between fold increase in IL-6R expression cells and increasing viral load, suggesting that KSHV infection led to upregulation of this receptor.

These results suggested that KSHV might confer enhanced potential reactivity to the proliferative signal, IL-6, on infected IgMλ B cells. This change would be consistent with the potential role of KSHV in driving differentiation of susceptible B cells toward a plasmablast phenotype, since normal human plasmablast differentiation involves IL-6 signaling (51). To test the functionality of the KSHV-induced increases in IL-6R expression, we added exogenous IL-6 to cultures following KSHV exposure and assessed the cells for growth at 72 hpi as we had earlier (Figure 4). IL-6 treatment resulted in a nearly 2-fold increase in the percentage of LANA⁺ cells that were blasting compared with no treatment (Figure 7E). We did not detect a significant difference in the percentage of dividing cells in most tonsil cultures at 72 hpi, but we cannot rule out the possibility that division would be similarly affected with different doses of IL-6 or at further time points after infection. These data supported our observations that KSHV induced a plasmablast phenotype in infected B cells and suggested that IL-6 acted as a growth factor for KSHV-infected cells.

Discussion
The genotypic and phenotypic characteristics of tumor cells reflect their origins, particularly for B cell neoplasms, in which transformation can halt cellular differentiation, leading to characteristic morphology, Ig rearrangements, and protein expression patterns

that are reminiscent of their pre-transformation phenotype (24). As a result, cancer biologists have made substantial efforts toward elucidating the "normal" counterpart for many B cell tumors to understand how these cells became transformed (reviewed in ref. 25). For the KSHV-associated B cell neoplasms PEL and MCD, studies examining the above cellular characteristics have allowed investigators to deduce the particular stage of B cell differentiation at which the transforming insult(s) might have occurred (4, 52). In the present study, we sought to complement this deductive approach by identifying the original cell type most likely targeted by KSHV and capable of sustaining infection. Better characterization of this B cell subset, we reasoned, would shed light on mechanisms of both viral transmission and tumorigenesis.

KSHV targets the IgMλ subset of tonsillar B cells. Rather than inferring the normal counterpart, we asked whether KSHV would stably infect a particular cellular subtype among a heterogeneous population of human tonsillar cells cultured ex vivo. Our results revealed that KSHV selectively established latent (LANA⁺) infection nearly exclusively in IgMλ B cells, a subpopulation that constitutes approximately 20% or less of human tonsils. In the conditions of our ex vivo experiments, we found, on average, evidence of LANA⁺ infection in approximately 1 in 25 of these IgMλ B cells within a given tonsil. Although we were unable in this study to determine the qualities that might distinguish more precisely this smaller subgroup of KSHV-susceptible cells, we empirically noted an association between small tonsils and low/absent latent (LANA⁺) KSHV infection. Since the tonsils that we obtained were deidentified, we had no patient data pertaining to potentially different inflammatory (e.g., bacterial tonsillitis) states. Nevertheless, this simple observation led us to speculate that an activated inflammatory state might increase susceptibility to LANA⁺ infection. We will be investigating this possibility in another cohort in which we will also have access to additional clinical data. Other factors that might explain why we detected LANA⁺ infection in only a small fraction of the IgMλ population could include increased susceptibility at different stage(s) of the cell cycle or among a highly specialized subepithelial subtype of IgMλ cells (see below). Significantly, we did not find evidence of latent (LANA⁺) infection in the non-B cells (mainly T cells) that constituted 30%–50% of the tonsillar cells in our cultures.

We are aware of no studies establishing phenotypic differences conferred by λ versus κ light chain expression, much less suggesting why KSHV might target the λ over the κ subset for latent (LANA⁺) infection. Ongoing studies in our laboratory are investigating potential biological differences between these cell types. Of interest, however, we did find evidence of a bystander effect of KSHV infection on λ B cells, where approximately 30% of these cells were proliferative but only 4%, on average, were LANA⁺. Attygalle et al. also described proliferation of λ B cells in atypical tonsillar hyperplasia in the absence of KSHV infection (P.G. Isaacson, unpublished observation, and ref. 53). In contrast to EBV and the related murine virus MHV-68 (54), KSHV binding alone did not appear sufficient to induce B cell activation and proliferation, since we found that UV-inactivated virus was unable to induce similar proliferation, although we did not directly assess whether UV treatment might have affected binding. It is formally possible that the increased proliferation of LANA⁻ λ B cells resulted from pre-latent (LANA dot–negative) infection. Since KSHV entry and pre-latent transcription (e.g., *PAN*) is evident throughout the culture, proliferation within LANA⁻ λ B cells might indicate that only λ B cells are able to respond to a component of this program. Alternatively, λ B cells might have enhanced sensitiv-

ity to a paracrine effect resulting from KSHV infection of neighboring cells. Our preliminary data (not shown) suggest that λ B cells, in general, have a higher propensity to proliferate than κ B cells. The potential role of this proliferative response in the establishment of KSHV latent infection within B cells is the subject of ongoing research in our laboratory.

In contrast to a previous report by Rappocciolo et al. in which KSHV infection of primary human B cells led to a 7-fold increase in intracellular virions and secretion of approximately 60 virions/B cell (17), we did not detect appreciable release of infectious virions or KSHV genomic DNA in the supernatant of infected tonsillar B cells. Similarly, we saw no increase in the intracellular levels of virus following infection. There are a number of key experimental differences between this earlier study and ours that might account for these distinct outcomes. First, Rappocciolo et al. isolated CD19-expressing B cells by positive selection. We chose negative selection (Figures 1 and 2) or none at all (Figure 3–7) to minimize potential signaling events from CD19 ligation (55) that might, in turn, alter the phenotype of the cells prior to or after KSHV infection. Second, Rappocciolo et al. used peripheral blood B cells preactivated for 36 hours by CD40L and IL-4 for most of their work, while we used exclusively tonsillar cells, omitting CD40L and IL4 pretreatment. We focused on tonsil-derived B cells, as we believe that they may represent the original target of KSHV transmitted via saliva. Third, it is possible that our tonsil donors represent distinct clinical subpopulations with varying susceptibility to KSHV infection. Finally, while Rappocciolo et al. show nearly 100% viability maintained over 72 hpi, we found a drop in viability to 50% by the same time, consistent with other reports (40). We speculate that this viability difference might reflect the effects of survival signals provided by CD40L and IL-4 activation in the Rappocciolo et al. study. Nevertheless, the differences in the two sets of findings underscore the importance of studying the role of activation signals in priming B cells for latent versus lytic infection.

KSHV infection and plasmablast differentiation. In addition to proliferation, our data suggested that KSHV infection drove differentiation of infected B cells toward a plasmablast phenotype highly reminiscent of MCD. The de novo infected B cells in our study were blasting, had an increased N/C ratio, and expressed high levels of IgMλ, as well as CD27, Ki67, and IL-6R. Previous studies have shown that IL-6 can promote growth (51), differentiation (56, 57), and survival (58, 59) of normal plasmablasts. Consistent with these biological roles, IL-6 treatment of de novo infected tonsillar B cells also resulted in enhanced blasting of LANA+ B cell that surpassed the baseline effect of KSHV infection alone. As this study, a snapshot at 72 hpi, revealed significant changes only in the percentage of cells with blasting morphology, we could not determine whether IL-6 was also capable of inducing further proliferative changes. Future kinetic and IL-6 dosage effect studies could provide more insight into this issue. Since clinical studies to date have demonstrated only that the systemic high levels of IL-6 present in MCD are responsible for clinical symptoms, this is the first documentation, to our knowledge, of the effect of IL-6 on KSHV-infected B cells other than PEL. This finding supports the hypothesis (3, 60, 61) that the lymphoproliferation of KSHV-infected cells in MCD may be IL-6–driven.

Our findings revealed that KSHV infection drove IgMλ tonsillar B cells to proliferate, as predicted by the Du et al. study, which indicated that MCD plasmablasts lack evidence of clonal expansion, except in rare progressive instances of frank lymphoma (3). We further showed that KSHV infection drove B cell differentiation to the plasmablast stage, as also suggested by Du et al. (3).

IgM memory B cells are the likely target of KSHV latent infection. Analysis by Du et al. also revealed that KSHV-infected cells carry few somatic Ig mutations and lack biased usage of Ig heavy- or light-chain family members that, if present, would have suggested expansion of cells in a GC reaction (3, 62). Most PELs examined to date are predominantly EBV-coinfected and show evidence of somatic hypermutation (SHM) and often class switching, indicating that they most likely derive from a GC-experienced cell. However, the EBV- PEL line (BC-3) displayed no SHM, indicating that they, like MCD B cells, likely derive from a GC-inexperienced B cell (63). Furthermore, previous work has shown that EBV-/KSHV+ PEL cells can express the λ light chain (4), and, according to our unpublished observation, at least one EBV- PEL line, BCBL-1, expresses IgM as well. It is therefore tempting to speculate that, in the absence of EBV infection, KSHV may also drive PEL formation from a GC-inexperienced, IgMλ B cell.

Previously, IgM+ B cells that lacked evidence of somatic hypermutation were assumed to be naive, and, prior to the present study, most characterizations of KSHV-infected neoplasms have concluded with the prediction that KSHV might originally target naive B cells for infection. While we do not have direct experimental evidence to the contrary, recent descriptions of a newly defined B cell subset suggest an alternative hypothesis. This subset, termed IgM memory B cells, is present in the spleen, blood, and tonsil and shares phenotypic similarities with murine marginal zone B cells (64–66). IgM memory B cells provide an immediate line of defense against pathogens by rapidly proliferating and secreting antibody after stimulation by oral or blood-borne pathogens. This propensity for activation and proliferation makes them a potentially attractive target for a virus that utilizes host cell division as a means of propagation. Furthermore these cells can circulate throughout the body (65), providing a potential modality for KSHV to spread to other sites within the host. IgM memory B cells express CD27 and high levels of IgM, and, in contrast to class-switched memory B cells, Ig gene sequencing of IgM memory B cells reveals that a portion of this population has unmutated Ig genes (65), as do MCD plasmablasts. IgM memory B cells are also located in the subepithelial region of the tonsil (67), the same region where Chagas et al. consistently found evidence of KSHV infection (21). Interestingly, this subset represents approximately 1%–2% of tonsillar B cells (67), a number close to the frequency of infection that we find in ex vivo tonsil cell suspensions.

Chadburn et al. found that KSHV-infected cells in MCD and PEL lesions express a transcription factor profile (PRDM1+, IRF4+Bcl-6- Pax5-) that indicates the cells are pre-terminally differentiated plasmablasts (4). Jourdan et al. (68) recently found that a similar transcription factor profile developed during in vitro differentiation of memory B cells (IgM memory and class-switched memory) into plasmablasts. In their system, a significant fraction of the memory B cells reached the early or late plasmablast stage by the fourth day of culture, concomitant with upregulation of IgM, a high level of Ki67 expression, and loss of CD27 expression on a fraction of the cells (68). These findings indicate that IgM memory B cells become IgMhi, Ki67+, and variably CD27+ during plasmablast differentiation and suggest that the KSHV-infected plasmablasts present in MCD lesions, as well as in the cultures in the present study, could derive from IgM memory B cells, rather than naive B cells. If the tar-

get of latent KSHV infection in tonsillar cultures were IgM memory B cells, and the virus were able to provide NF-κB signals that substitute for those the B cell normally requires for differentiation (as previous studies have suggested; refs. 69–73), it is conceivable that infected cells would show an early plasmablast phenotype 3–4 days after exposure to KSHV-infection — an observation we have made in this study. The alternative model involving KSHV infection of naive B cells is less attractive, since plasmablast differentiation from this early stage would likely not be evident by 72 hpi (74). Furthermore, the lack of association between CD27 levels and increased viral load in our study argues against the alternative, which would be upregulation of CD27 on a naive B cell infected by KSHV.

Definitive determination of whether KSHV specifically targets IgM+CD27+ memory B cells, as opposed to inducing CD27 expression on naive B cells, would require side-by-side exposure of sorted CD27+ and CD27- B cells from the same tonsil, followed by direct comparison of infection rates. This experiment would require ligation of the B cell receptor (IgM), which activates B cells, as well as CD27 ligation, which may be involved in plasma cell differentiation (75). While future work in our laboratory will concentrate on this type of investigation, in the current study we purposely focused on characterizing KSHV infection in a minimally manipulated tonsillar B cell system, potentially avoiding the confounding effects of activation on KSHV tropism and B cell post-infection phenotype.

Based on (a) the location of KSHV+ cells in the subepithelial region of human tonsils (21), (b) the phenotypic subtleties shared by MCD B cells (3, 4, 62), ex vivo infected tonsillar B cells, and the recently described IgM memory B cells (65, 68, 76), and (c) the similar frequencies of tonsillar IgM memory B cells (67) and KSHV-susceptible tonsillar B cells, we hypothesize that KSHV latently infects IgM memory B cells derived from the subepithelial region of the tonsil, rather than naive B cells. B cells with a memory phenotype are preactivated and primed to quickly respond to potential pathogen signals by proliferating and further differentiating into antibody-secreting cells. Infection of this cell type would provide a latent virus with an immediate means of amplification (through cellular proliferation) and dissemination (via circulation of these cells throughout the host) as well as facilitating the eventual production of virions (by XBP-1 induction) if and when the cell terminally differentiated into a plasma cell (52, 77, 78).

Intracellular viral load and degree of B cell differentiation. Based on lower expression of Ki67 and the presence of obvious surface Ig, we found the de novo infected B cells at 3–4 dpi to be slightly less differentiated than MCD plasmablasts, which contain primarily cytoplasmic Ig and are more proliferative (68). MCD plasmablasts are, in turn, less differentiated than PEL cells, which express the plasma cell marker CD138 and contain no surface Ig. Therefore, we propose a spectrum for KSHV-infected B cell differentiation that positively correlates with intracellular viral load, where de novo infected B cells are the least terminally differentiated and contain the fewest number of viral genomes, evidenced by the low number of LANA dots/cell (mean of 1.7 dots/cell in our study); MCD B cells are then intermediate in both parameters (79); and PEL are the most differentiated, as well as highly transformed, and have the highest intracellular viral load (79). In support of this theory, we found a correlation within de novo infected tonsillar B cells between intracellular viral load (LANA dots/cell) and plasmablast markers (IgMhi, Ki67, IL-6R) expressed on MCD B cells. This correlation suggests that KSHV infection drives B cell differentiation toward the plasma cell stage. Since full plasma cell differentia-

tion, and accompanying XBP-1 expression, however, would likely drive KSHV infection from latency to lytic replication (77, 78), we predict that KSHV employs a mechanism for controlling the final stages of plasma cell differentiation in order to maintain a latent state during most of its life cycle.

Methods

Cell culture and KSHV preparation. KSHV-positive BCBL-1 cells were grown at 37°C and 5% CO_2 in RPMI medium supplemented with RPMI 1640 media (GIBCO, Invitrogen) and 10% FBS, 10 mM HEPES (pH 7.5), 100 U/ml penicillin, 100 μg/ml streptomycin, 2 mM L-glutamine, 0.05 mM β-mercaptoethanol, and 0.02% (wt/vol) sodium bicarbonate as previously described (80). HeLa cells (ATCC) were grown in DMEM (GIBCO) supplemented with penicillin-streptomycin and 10% fetal bovine serum. KSHV virion production in BCBL-1 cells was induced with 0.6 μM valproic acid (2-propylpentanoic acid). Seven to 8 days after induction, KSHV virions were purified by centrifugation as described previously (80). In brief, virus was concentrated by centrifugation through 20% sucrose in TNE (10 mM Tris [pH 7.4], 200 mM NaCl, 1 mM EDTA pH 7.4) cushion (17,696 g for 3 hours in a Sorvall SLA-3000 rotor) from media precleared of cellular debris. Infectious titer was determined as LANA dot–forming units by serial dilution infection of HeLa cells in the presence of Polybrene as previously described (39). Inactivated KSHV was prepared by incubating viral stocks with 10 mJ/cm² UV light for 10 minutes as previously described (39).

Isolation of tonsillar cells. Deidentified tonsils were obtained from the Biorepository and Tissue Research Facility following routine tonsillectomy of patients at the University of Virginia medical center. The use of deidentified samples is exempt from review by the IRB of the University of Virginia. Necrotic and cauterized tissue was removed, and viable tonsil tissue was cut into pieces approximately 200 mm × 200 mm and teased apart to release tonsillar cells in a solution of 1× PBS/2% FBS/2 mM EDTA. The suspension of 2×10^9 cells was passed through a size 60 mesh screen, washed, and centrifuged over Lympholyte-H (Cedarlane Labs) to isolated viable cells. Cells were immediately exposed to KSHV (or UV-KSHV) and cultured or were cryopreserved in a solution of 10% DMSO, 30% FBS, 60% RPMI. For isolation of B cells, tonsil suspensions were incubated with 150 ml RosetteSep B Cell Enrichment Cocktail (Stem Cell Inc.), 450 ml RosetteSep CD3 Depletion Antibody Cocktail (Stem Cell Inc.), and approximately 2×10^{10} heterologous red blood cells for 20 minutes before centrifugation over RosetteSep-DM media. Cells were washed and remaining red blood cells lysed at 37°C for 5 minutes with ACK lysis buffer (0.15 M NH$_4$Cl, 10 mM KHCO$_3$, 0.1 mM Na$_2$EDTA in distilled H$_2$O), washed again, and used immediately or cyropreserved.

Infection and culture of tonsillar cells. Tonsil cell suspensions or isolated B cell suspensions at 1×10^7 cells/ml were incubated for 2 hours at 37°C with 5×10^7 to 1×10^8 infectious units of KSHV/ml in RPMI/2% FBS, resulting in an MOI of 5–10. For most experiments, the KSHV inoculum was left in the media, and complete RPMI for primary cells (without β-ME, containing 5 mg/ml amphotericin B [Invitrogen]) was added to achieve a final cell concentration of 2×10^6/ml. IL-2 (Tecin, AIDS Research and Reference Reagent Program NIAID, NIH) and IL-4 (R&D Systems) were added at final concentrations of 10 U/ml and 100 U/ml, respectively. For experiments quantifying KSHV genomic DNA and RNA, cells were washed 3 times with 5 volumes 2% FBS/RPMI before being resuspended in complete B cell media. In some experiments, IL-6 (R&D Systems) was also added 12–18 hpi at a final concentration of 40 ng/ml. For DNA and RNA experiments, cryopreserved cells were thawed and rested at least 4 hours before exposure to KSHV and infected at an MOI of 10. For all immunostaining experiments, freshly isolated tonsillar cells were used to minimize autofluorescence and infected at an MOI of 5 to conserve viral preparations. For long-term culture of B cells after KSHV infection (or

Table 1

Primers and probes

Primer/probe	Sequence
qORF73F	5′-TACTTTACCGGTGGCTCCCA-3′
qORF73R	5′-GGGTAAGAGTGCCGGTGGA-3′
qORF73probe	5′-FAM-CACCCGCTCCCGCAACACCTTTAC-BHQ1-3′
qHuGAPDH_120F	5′-GAAGATGGTGATGGGATTTCCA-3′
qHuGAPDH_203R	5′-GATTCCACCCATGGCAAATT-3′
qPAN-RNA-F	5′-TCTGCTCATTCGTTGTTTCG-3′
qPAN-RNA-R	5′-GCTTCACAACGCACCAATAA-3′
qPAN-probe	5′-FAM-CGGATTGAGTGTAAATCGGG-BHQ1-3′

mock infection), cultures were transferred onto a layer of CD40L-transfected NIH-3T3 fibroblasts (gift from Eugene Barsov, NIH/National Cancer Institute, Bethesda, Maryland, USA) that had been treated for 2 hours with 4 mg/ml mitomycin C (Roche).

Quantification of cell-associated and internalized KSHV genomes. After incubation of cells with KSHV at an MOI of 10 for 2 hours, 5 volumes RPMI/2% FBS was added, and the cells were centrifuged at 300 *g* for 8 minutes. Cells were then washed 3 times with 5 volumes of RPMI/2% FBS and then cultured in complete RPMI for primary cells for the remainder of the experiment, or, to quantify internalized KSHV, surface-bound virus was removed by treatment of cells with 0.25% trypsin/2.69 mM EDTA at 37°C for 5 minutes (36). Cells were then washed twice with 5 volumes of serum-free RPMI before DNA was extracted and amplified by qPCR.

Total DNA was extracted from 1×10^6 human tonsillar B cells by overnight digestion with proteinase K, followed by phenol-chloroform extraction and ethanol precipitation, with glycogen carrier to aid recovery (Glycoblue, Ambion). KSHV genomic copy numbers were assayed in triplicate by real-time PCR (Taqman Universal PCR Master Mix, Applied Biosystems) using primers and hydrolysis probe specific to the ORF73 coding sequence, as detected by an ABI Prism 7900 HT instrument at the University of Virginia Biomolecular Research Center. Quantification was based on serial dilution of a plasmid bearing the ORF73 coding sequence, pcDNA3-LANA. Approximately 35 ng of total DNA was assayed per reaction, as estimated by absorbance at 260 nm, and all samples were normalized for total input based on a parallel assay using primers specific for the human *GAPDH* coding sequence, and SYBR dye for visualization (SYBR Green PCR Master Mix, Applied Biosystems). Relative *GAPDH* levels were then used to gener-

ate a normalization factor for each extracted DNA sample relative to the average for the experiment. Normalized KSHV genomes per 35 ng of total extracted DNA were then further converted to relative copies per 1,000 cells by an estimate of 9 pg of genomic DNA per cell (81–83). Standard deviation of the absolute viral genome copy number across triplicate wells was propagated through these normalization calculations. Primers and probes used in these assays were synthesized commercially (Eurofins MWG Operon, Biosearch Technologies Inc.) and are listed in Table 1.

Quantification of KSHV RNA. Total RNA was extracted from 5×10^6 human tonsillar B cells using Tri-Reagent (Ambion) in accordance with the manufacturer's protocol. Residual DNA was removed from samples by treatment with TURBO-DNAse (Ambion), and 0.5–1.0 μg total RNA per condition was converted to first-strand cDNA using oligo-dT primers by means of the RETROscript reverse transcription kit (Ambion), according to the manufacturer's protocol. Diluted cDNA equivalent to 5–20 ng of total input RNA, or equivalent no-RT controls, was assayed in triplicate by quantitative real-time PCR on an ABI Prism 7900HT instrument (Applied Biosystems). Specific viral transcripts were detected by hydrolysis probes (Taqman Universal Master Mix, Applied Biosystems), using primers and probes listed in Table 1. Quantification was based on standard curves of plasmids bearing the target DNA sequences (qPCR-TOPO-PAN, qPCR-TOPO-h*GAPDH*, pcDNA3-LANA). All *PAN* transcript levels were normalized to *GAPDH*, as assayed from dilutions of the same cDNA templates, but utilizing a DNA dye-based detection (SYBR-Green PCR Master Mix, Applied Biosystems).

Immunostaining. To identify cells that were viable at the time of collection, cells were pretreated with 200 mg/ml DNase I for 20 minutes (41) before fixation with 3% freshly opened methanol-free formaldehyde/0.03 M sucrose for 15 minutes at room temperature. Cells were washed with PBS and permeabilized with ice-cold MeOH for 10 minutes on ice. After washing with PBS, staining was performed in staining buffer (1% fetal calf serum, 0.09% sodium azide in PBS) at room temperature. Nonspecific staining was blocked with 5 mg/ml purified rat IgG (SouthernBiotech). Cells were labeled at room temperature with antibodies listed in Table 2. When anti-κ (SouthernBiotech) was used, cells were labeled with anti-λ in a separate step to avoid cross-reactivity. Cells were washed twice and resuspended in PBS with 0.1 mg/ml DAPI for 5 minutes. Cell suspensions were filtered and resuspended in PBS before analysis by MIFC (Imagestream-100, Amnis).

MIFC. MIFC was performed by collecting 50,000 events per sample to identify LANA dot⁺ cells as previously described (27) with modifications. The new EDF modification (31) was used for all analyses. Table 3

Table 2

Antibodies and fluorophores used for MIFC

Target channel	Fluorophore	Source	Species	Dilution	Imagestream
LANA	Alexa Fluor 488 (conjugated, Molecular Probes)	Advanced Biotechnologies Inc.	Mouse IgG1	1:1,500	Channel 3
λ	Biotin	SouthernBiotech	Goat F(ab)₂	1:400	Channel 6
Streptavidin	Alexa Fluor 647	Molecular Probes		1:500	Channel 6
κ	PE	SouthernBiotech	Goat F(ab)₂	1:100	Channel 4
κ	PE	BD	Mouse IgG₁	1:100	Channel 4
CD27	PE	Invitrogen	Mouse IgG₂ₐ	1:20	Channel 4
IgM	Alexa Fluor 647	Molecular Probes	Goat	1:100	Channel 6
IL-6R	Biotin	eBioscience	Mouse IgG₁	1:20	Channel 5
Streptavidin	PE–Texas red	Invitrogen		1:500	Channel 5
Ki67	Alexa Fluor 647	eBioscience	Mouse IgG₁κ	1:20	Channel 6
Nuclei	DAPI	Sigma-Aldrich		0.5 mg/ml	Channel 2

Table 3
Description of MIFC parameters

Parameter	IDEAS feature	Detail
Single cells	Area_Ch1	<300 μm²
Single cells	Aspect_Ratio_Ch1	0.45–1
Focused cells	Gradient_RMS_Ch5	200–400
Focused cells	Contrast_Ch5	<20
Viable cells	Intensity_Ch2	DAPI bright population chosen
Single nuclei	Aspect_Ratio_Intensity_Ch2	0.6–1
LANA dots	Nuclear mask	Morphology mask of DAPI image, or DAPI image mask eroded by 1 pixel
LANA dots	Spot mask	Bright; spot/cell background, 7–10; radius, 3–4
LANA dots	Peak mask	Spot/cell background, 1.5–2
LANA dots	Range mask	Area, <15 μm²
LANA dots	Spot count	For spots defined by combining above 4 mask features into 1 mask
LANA spots	Intensity_MC_Ch3	>500
DNA content	Intensity_M2_Ch2	Individual values vary, 1× and 2× populations
Cell size/area	Bright-field mask (M5)	Area_M5
N/C ratio	DAPI images mask	Area_M2
N/C ratio	"Cytoplasm mask"	Bright-field mask (M5) and not nuclear mask
N/C ratio	Cytoplasm area	Area_"Cytoplasmic mask"
N/C ratio	Combined feature mask	Area_M2/Area_"cytoplasmic mask"

lists all parameters measured in this study, the IDEAS software (Amnis) feature(s) used, and further details about inclusion of cells or measurement of values within that feature. IDEAS 3.0 was used to analyze all samples. Actual images and data plots, however, were generated using IDEAS 4.0 for improved resolution.

The Intensity feature measures the sum of the background-subtracted pixel values within an area of an individual image. Intensity features are given with the mask to which they are confined. For example, Intensity_MC_Ch3 is the intensity of background-subtracted pixels detected in channel 3 within the MC, or combined, whole cell mask. Default masks are represented by M, with MC representing a combined mask for all measured parameters, whereas numbers (e.g., M2) represent masks based on signal from a specific channel (e.g., channel 2).

To identify single cells, we plotted area by aspect ratio of channel 1, which is a parameter similar to side scatter in conventional flow cytometry. Area is equal to the number of micrometers squared in a given mask. To determine area, IDEAS software converts the number of pixels to μm² (1 pixel = 0.25 μm²). Aspect ratio describes the shape of a cell is and is the ratio of the longest to the shortest dimensions of a best-fit ellipse drawn around the image. We drew a gate around cells as described in Table 3 and visually inspected the cells that we had included to confirm that they were, in fact, nearly all single cells.

To isolate cells that were in focus, we plotted the gradient root mean squared (RMS) × contrast of the bright-field images. Both features measure the sharpness of an image based on detection of large pixel value changes, but they use different weighted assignments to the pixel arrays to do so. We drew a gate around cells as described in Table 3 and visually inspected the cells that we had included to confirm their image quality.

To identify viable cells, we plotted the intensity of the DAPI signal by the aspect ratio of DAPI intensity (the latter of which further assisted in elimination of doublets). Because nonviable cells were permeable to DNase, they stained dimly with DAPI and were easily discernible from the brighter viable cells. We drew a gate around cells as described in Table 3.

To determine the number of LANA spots/cell, we applied the IDEAS Spot Count feature to a combined mask that was based on a nuclear mask, which defined the area of interest and excluded any potential non-nuclear signal. We then added a spot mask to the nuclear mask. Spot masks are initially created by IDEAS software by an image-processing step that erodes all but the brightest areas of an image and are then refined by the user. For LANA dots, we chose to define spots as at least 7-fold brighter than background and having a radius of 3 pixels or greater. We then applied a peak mask to the spot mask, which identifies areas in the image with local bright maxima and set a spot/background criteria of 1.5 or 2, depending on the experiment. This feature helps resolve adjacent spots. For some analyses, we further defined the spot mask with a range mask to exclude spots greater than 15 μm², although the improvement upon spot counting without the range mask was minimal. We then plotted the spot count by the intensity of LANA signal and gated all cells that had at least one spot and had greater than 500 intensity units, calling them LANA⁺. The final combined spot mask and spot counting were tested for accuracy by visual inspection of this LANA⁺ population. In some experiments, the spot masks were altered very slightly as represented in Table 3 to more rigorously define spot size, spot/background ratio, or nuclear area. This was done to reduce background signal in cultures that were not treated with KSHV, and the modified algorithm was applied to the corresponding KSHV-exposed samples to maintain a consistent measure within independent experiments.

To determine the N/C ratios for individual cells, we created our own "cytoplasmic mask" by subtracting the nuclear mask from the entire bright-field image mask. We then created a combined feature to divide the area of the nuclear mask by the area of the cytoplasmic mask to give a single value for each cell. We report the mean values for each population of cells in our results.

Assessment of proliferation by EdU incorporation. 2×10^6 KSHV-exposed or unexposed tonsillar cells/ml were cultured in 24-well plates in the presence of 2 μM of the nucleoside analog EdU (Invitrogen). At the time of harvest, cells were treated with DNase as described above and fixed with 3% methanol-free formaldehyde for 20 minutes. Cells were washed with PBS and permeabilized with ice-cold 100% MeOH. After washing with PBS containing 1% BSA and 0.09% sodium azide, cells were labeled with 200 μl Click-IT Pacific Blue Reaction cocktail (Invitrogen) for 30 minutes. After washing, cells were additionally labeled with FITC-conjugated anti-λ (BD) and PE-conjugated anti-κ (BD) antibodies for 30 minutes. After washing, cells were incubated with 500 mg/ml RNase A and 25 mM DRAQ5 (BioStatus Ltd.) and run on a CyAn ADP 9 Color flow cytometer (Beckman Coulter).

Statistics. Paired, 1-tailed *t* tests were performed on all matched samples, and *P* values indicate results of paired *t* test analysis except where otherwise indicated. For analyses with more than 2 groups, we used either 1-way ANOVA or, for analysis of correlation between increasing viral load and cellular phenotype, a Spearman correlation test. The results of these last two types of analyses are stated in the legends. For all analyses, *P* values less than 0.05 are given. *P* values greater than 0.05 were considered insignificant.

1. Waterston A, Bower M. Fifty years of multicentric Castleman's disease. *Acta Oncol*. 2004;43(8):698–704.
2. Carbone A, Gloghini A. KSHV/HHV8-associated lymphomas. *Br J Haematol*. 2008;140(1):13–24.
3. Du MQ, et al. Kaposi sarcoma-associated herpesvirus infects monotypic (IgM lambda) but polyclonal naive B cells in Castleman disease and associated lymphoproliferative disorders. *Blood*. 2001;97(7):2130–2136.
4. Chadburn A, et al. Immunophenotypic analysis of the Kaposi sarcoma herpesvirus (KSHV; HHV-8)-infected B cells in HIV+ multicentric Castleman disease (MCD). *Histopathology*. 2008;53(5):513–524.
5. Judde JG, et al. Monoclonality or oligoclonality of human herpesvirus 8 terminal repeat sequences in Kaposi's sarcoma and other diseases. *J Natl Cancer Inst*. 2000;92(9):729–736.
6. Brandt SJ, Bodine DM, Dunbar CE, Nienhuis AW. Dysregulated interleukin 6 expression produces a syndrome resembling Castleman's disease in mice. *J Clin Invest*. 1990;86(2):592–599.
7. Katsume A, et al. Anti-interleukin 6 (IL-6) receptor antibody suppresses Castleman's disease like symptoms emerged in IL-6 transgenic mice. *Cytokine*. 2002;20(6):304–311.
8. Matsuyama M, et al. Anti-interleukin-6 receptor antibody (tocilizumab) treatment of multicentric Castleman's disease. *Intern Med*. 2007;46(11):771–774.
9. Kawabata H, Tomosugi N, Kanda J, Tanaka Y, Yoshizaki K, Uchiyama T. Anti-interleukin 6 receptor antibody tocilizumab reduces the level of serum hepcidin in patients with multicentric Castleman's disease. *Haematologica*. 2007;92(6):857–858.
10. Taniguchi K, et al. Tocilizumab is effective for pulmonary hypertension associated with multicentric Castleman's disease. *Int J Hematol*. 2009;90(1):99–102.
11. Gaidano G, et al. Association of Kaposi's sarcoma-associated herpesvirus-positive primary effusion lymphoma with expression of the CD138/syndecan-1 antigen. *Blood*. 1997;90(12):4894–4900.
12. Cesarman E, Knowles DM. The role of Kaposi's sarcoma-associated herpesvirus (KSHV/HHV-8) in lymphoproliferative diseases. *Semin Cancer Biol*. 1999;9(3):165–174.
13. Cesarman E, Chang Y, Moore PS, Said JW, Knowles DM. Kaposi's sarcoma-associated herpesvirus-like DNA sequences in AIDS-related body-cavity-based lymphomas. *N Engl J Med*. 1995;332(18):1186–1191.
14. Soulier J, et al. Kaposi's sarcoma-associated herpesvirus-like DNA sequences in multicentric Castleman's disease. *Blood*. 1995;86(4):1276–1280.
15. Chang Y, et al. Identification of herpesvirus-like DNA sequences in AIDS-associated Kaposi's sarcoma. *Science*. 1994;266(5192):1865–1869.
16. Ambroziak JA, et al. Herpes-like sequences in HIV-infected and uninfected Kaposi's sarcoma patients. *Science*. 1995;268(5210):582–583.
17. Rappocciolo G, et al. Human herpesvirus 8 infects and replicates in primary cultures of activated B lymphocytes through DC-SIGN. *J Virol*. 2008; 82(10):4793–4806.
18. Mesri EA, et al. Human herpesvirus-8/Kaposi's sarcoma-associated herpesvirus is a new transmissible virus that infects B cells. *J Exp Med*. 1996;
183(5):2385–2390.
19. Mayama S, et al. Prevalence and transmission of Kaposi's sarcoma-associated herpesvirus (human herpesvirus 8) in Ugandan children and adolescents. *Int J Cancer*. 1998;77(6):817–820.
20. Vieira J, Huang ML, Koelle DM, Corey L. Transmissible Kaposi's sarcoma-associated herpesvirus (human herpesvirus 8) in saliva of men with a history of Kaposi's sarcoma. *J Virol*. 1997;71(9):7083–7087.
21. Chagas CA, Endo LH, Sakano E, Pinto GA, Brousset P, Vassallo J. Detection of herpesvirus type 8 (HHV8) in children's tonsils and adenoids by immunohistochemistry and in situ hybridization. *Int J Pediatr Otorhinolaryngol*. 2006;70(1):65–72.
22. Takizawa M, Sugane K, Agematsu K. Role of tonsillar IgD+CD27+ memory B cells in humoral immunity against pneumococcal infection. *Hum Immunol*. 2006;67(12):966–975.
23. Jendholm J, Samuelsson M, Cardell LO, Forsgren A, Riesbeck K. Moraxella catarrhalis-dependent tonsillar B cell activation does not lead to apoptosis but to vigorous proliferation resulting in nonspecific IgM production. *J Leukoc Biol*. 2008;83(6):1370–1378.
24. Salmon SE, Seligmann M. B-cell neoplasia in man. *Lancet*. 1974;2(7891):1230–1233.
25. Sagaert X, Sprangers B, De Wolf-Peeters C. The dynamics of the B follicle: understanding the normal counterpart of B-cell-derived malignancies. *Leukemia*. 2007;21(7):1378–1386.
26. Kuppers R, Klein U, Hansmann ML, Rajewsky K. Cellular origin of human B-cell lymphomas. *N Engl J Med*. 1999;341(20):1520–1529.
27. Adang LA, Parsons CH, Kedes DH. Asynchronous progression through the lytic cascade and variations in intracellular viral loads revealed by high-throughput single-cell analysis of Kaposi's sarcoma-associated herpesvirus infection. *J Virol*. 2006;80(20):10073–10082.
28. Fejer G, Medveczky MM, Horvath E, Lane B, Chang Y, Medveczky PG. The latency-associated nuclear antigen of Kaposi's sarcoma-associated herpesvirus interacts preferentially with the terminal repeats of the genome in vivo and this complex is sufficient for episomal DNA replication. *J Gen Virol*. 2003;84(pt 6):1451–1462.
29. Ballestas ME, Chatis PA, Kaye KM. Efficient persistence of extrachromosomal KSHV DNA mediated by latency-associated nuclear antigen. *Science*. 1999;284(5414):641–644.
30. Garber AC, Hu J, Renne R. Latency-associated nuclear antigen (LANA) cooperatively binds to two sites within the terminal repeat, and both sites contribute to the ability of LANA to suppress transcription and to facilitate DNA replication. *J Biol Chem*. 2002;277(30):27401–27411.
31. Ortyn WE, et al. Extended depth of field imaging for high speed cell analysis. *Cytometry A*. 2007; 71(4):215–231.
32. Akula SM, Pramod NP, Wang FZ, Chandran B. Human herpesvirus 8 envelope-associated glycoprotein B interacts with heparan sulfate-like moieties. *Virology*. 2001;284(2):235–249.
33. Hurley EA, Thorley-Lawson DA. B cell activation and the establishment of Epstein-Barr virus latency.
J Exp Med. 1988;168(6):2059–2075.
34. Kedes DH, Ganem D. Sensitivity of Kaposi's sarcoma-associated herpesvirus replication to antiviral drugs. Implications for potential therapy. *J Clin Invest*. 1997;99(9):2082–2086.
35. Sun R, Lin SF, Gradoville L, Miller G. Polyadenylylated nuclear RNA encoded by Kaposi sarcoma-associated herpesvirus. *Proc Natl Acad Sci U S A*. 1996; 93(21):11883–11888.
36. Krishnan HH, Naranatt PP, Smith MS, Zeng L, Bloomer C, Chandran B. Concurrent expression of latent and a limited number of lytic genes with immune modulation and antiapoptotic function by Kaposi's sarcoma-associated herpesvirus early during infection of primary endothelial and fibroblast cells and subsequent decline of lytic gene expression. *J Virol*. 2004;78(7):3601–3620.
37. Cotter MA 2nd, Robertson ES. The latency-associated nuclear antigen tethers the Kaposi's sarcoma-associated herpesvirus genome to host chromosomes in body cavity-based lymphoma cells. *Virology*. 1999;264(2):254–264.
38. Schwam DR, Luciano RL, Mahajan SS, Wong L, Wilson AC. Carboxy terminus of human herpesvirus 8 latency-associated nuclear antigen mediates dimerization, transcriptional repression, and targeting to nuclear bodies. *J Virol*. 2000;74(18):8532–8540.
39. Parsons CH, et al. KSHV targets multiple leukocyte lineages during long-term productive infection in NOD/SCID mice. *J Clin Invest*. 2006; 116(7):1963–1973.
40. Giger B, et al. Human tonsillar tissue block cultures differ from autologous tonsillar cell suspension cultures in lymphocyte subset activation and cytokine gene expression. *J Immunol Methods*. 2004;289(1-2):179–190.
41. Frankfurt OS. Assessment of cell viability by flow cytometric analysis using DNase exclusion. *Exp Cell Res*. 1983;144(2):478–482.
42. von Bergwelt-Baildon MS, et al. Human primary and memory cytotoxic T lymphocyte responses are efficiently induced by means of CD40-activated B cells as antigen-presenting cells: potential for clinical application. *Blood*. 2002;99(9):3319–3325.
43. Taussig MJ. Molecular genetics of immunoglobulins. *Immunol Suppl*. 1988;1:7–15.
44. Hsu SM, Cossman J, Jaffe ES. Lymphocyte subsets in normal human lymphoid tissues. *Am J Clin Pathol*. 1983;80(1):21–30.
45. Hart DN, McKenzie JL. Isolation and characterization of human tonsil dendritic cells. *J Exp Med*. 1988;168(1):157–170.
46. Kelley-Clarke B, De Leon-Vazquez E, Slain K, Barbera AJ, Kaye KM. Role of Kaposi's sarcoma-associated herpesvirus C-terminal LANA chromosome binding in episome persistence. *J Virol*. 2009;83(9):4326–4337.
47. Ross W, Hall PA. Ki67: from antibody to molecule to understanding? *Clin Mol Pathol*. 1995; 48(3):M113–M117.
48. Jackson SM, et al. Key developmental transitions in human germinal center B cells are revealed by differential CD45RB expression. *Blood*. 2009; 113(17):3999–4007.

49. Nicholas J. Human herpesvirus 8-encoded proteins with potential roles in virus-associated neoplasia. *Front Biosci*. 2007;12:265–281.

50. Gasperini P, Sakakibara S, Tosato G. Contribution of viral and cellular cytokines to Kaposi's sarcoma-associated herpesvirus pathogenesis. *J Leukoc Biol*. 2008;84(4):994–1000.

51. Jego G, Bataille R, Pellat-Deceunynck C. Interleukin-6 is a growth factor for nonmalignant human plasmablasts. *Blood*. 2001;97(6):1817–1822.

52. Jenner RG, et al. Kaposi's sarcoma-associated herpesvirus-infected primary effusion lymphoma has a plasma cell gene expression profile. *Proc Natl Acad Sci U S A*. 2003;100(18):10399–10404.

53. Attygalle AD, et al. Atypical marginal zone hyperplasia of mucosa-associated lymphoid tissue: a reactive condition of childhood showing immunoglobulin lambda light-chain restriction. *Blood*. 2004;104(10):3343–3348.

54. Flano E, Woodland DL, Blackman MA. A mouse model for infectious mononucleosis. *Immunol Res*. 2002;25(3):201–217.

55. de Rie MA, Schumacher TN, van Schijndel GM, van Lier RA, Miedema F. Regulatory role of CD19 molecules in B-cell activation and differentiation. *Cell Immunol*. 1989;118(2):368–381.

56. Tarte K, et al. Generation of polyclonal plasmablasts from peripheral blood B cells: a normal counterpart of malignant plasmablasts. *Blood*. 2002;100(4):1113–1122.

57. Matsui W, Huff CA, Vala M, Barber J, Smith BD, Jones RJ. Anti-tumour activity of interferon-alpha in multiple myeloma: role of interleukin 6 and tumor cell differentiation. *Br J Haematol*. 2003; 121(2):251–258.

58. Spets H, Stromberg T, Georgii-Hemming P, Siljason J, Nilsson K, Jernberg-Wiklund H. Expression of the bcl-2 family of pro- and anti-apoptotic genes in multiple myeloma and normal plasma cells: regulation during interleukin-6(IL-6)-induced growth and survival. *Eur J Haematol*. 2002;69(2):76–89.

59. Jourdan M, De Vos J, Mechti N, Klein B. Regulation of Bcl-2-family proteins in myeloma cells by three myeloma survival factors: interleukin-6, interferon-alpha and insulin-like growth factor 1. *Cell Death Differ*. 2000;7(12):1244–1252.

60. An J, Lichtenstein AK, Brent G, Rettig MB. The Kaposi sarcoma-associated herpesvirus (KSHV) induces cellular interleukin 6 expression: role of the KSHV latency-associated nuclear antigen and the AP1 response element. *Blood*. 2002;99(2):649–654.

61. Oksenhendler E, et al. High levels of human herpesvirus 8 viral load, human interleukin-6, interleukin-10, and C reactive protein correlate with exacerbation of multicentric castleman disease in HIV-infected patients. *Blood*. 2000;96(6):2069–2073.

62. Dupin N, et al. HHV-8 is associated with a plasmablastic variant of Castleman disease that is linked to HHV-8-positive plasmablastic lymphoma. *Blood*. 2000;95(4):1406–1412.

63. Matolcsy A, Nador RG, Cesarman E, Knowles DM. Immunoglobulin VH gene mutational analysis suggests that primary effusion lymphomas derive from different stages of B cell maturation. *Am J Pathol*. 1998;153(5):1609–1614.

64. Dono M, et al. The human marginal zone B cell. *Ann N Y Acad Sci*. 2003;987:117–124.

65. Weller S, et al. Human blood IgM "memory" B cells are circulating splenic marginal zone B cells harboring a prediversified immunoglobulin repertoire. *Blood*. 2004;104(12):3647–3654.

66. Martin F, Kearney JF. Marginal-zone B cells. *Nat Rev Immunol*. 2002;2(5):323–335.

67. Dono M, et al. CD5+ B cells with the features of subepithelial B cells found in human tonsils. *Eur J Immunol*. 2007;37(8):2138–2147.

68. Jourdan M, et al. An in vitro model of differentiation of memory B cells into plasmablasts and plasma cells including detailed phenotypic and molecular characterization. *Blood*. 2009; 114(25):5173–5181.

69. Dadke D, Fryer BH, Golemis EA, Field J. Activation of p21-activated kinase 1-nuclear factor kappaB signaling by Kaposi's sarcoma-associated herpes virus G protein-coupled receptor during cellular transformation. *Cancer Res*. 2003;63(24):8837–8847.

70. Emuss V, Lagos D, Pizzey A, Gratrix F, Henderson SR, Boshoff C. KSHV manipulates Notch signaling by DLL4 and JAG1 to alter cell cycle genes in lymphatic endothelia. *PLoS Pathog*. 2009;5(10):e1000616.

71. Chiou CJ, et al. Patterns of gene expression and a transactivation function exhibited by the vGCR (ORF74) chemokine receptor protein of Kaposi's sarcoma-associated herpesvirus. *J Virol*. 2002; 76(7):3421–3439.

72. Guasparri I, Keller SA, Cesarman E. KSHV vFLIP is essential for the survival of infected lymphoma cells. *J Exp Med*. 2004;199(7):993–1003.

73. Chugh P, et al. Constitutive NF-kappaB activation, normal Fas-induced apoptosis, and increased incidence of lymphoma in human herpes virus 8 K13 transgenic mice. *Proc Natl Acad Sci U S A*. 2005; 102(36):12885–12890.

74. Huggins J, et al. CpG DNA activation and plasma-cell differentiation of CD27- naive human B cells. *Blood*. 2007;109(4):1611–1619.

75. Jacquot S, Kobata T, Iwata S, Morimoto C, Schlossman SF. CD154/CD40 and CD70/CD27 interactions have different and sequential functions in T cell-dependent B cell responses: enhancement of plasma cell differentiation by CD27 signaling. *J Immunol*. 1997;159(6):2652–2657.

76. Tangye SG, Good KL. Human IgM+CD27+ B cells: memory B cells or "memory" B cells? *J Immunol*. 2007; 179(1):13–19.

77. Dalton-Griffin L, Wilson SJ, Kellam P. X-box binding protein 1 contributes to induction of the Kaposi's sarcoma-associated herpesvirus lytic cycle under hypoxic conditions. *J Virol*. 2009; 83(14):7202–7209.

78. Yu F, Feng J, Harada JN, Chanda SK, Kenney SC, Sun R. B cell terminal differentiation factor XBP-1 induces reactivation of Kaposi's sarcoma-associated herpesvirus. *FEBS Lett*. 2007;581(18):3485–3488.

79. Parravicini C, et al. Differential viral protein expression in Kaposi's sarcoma-associated herpesvirus-infected diseases: Kaposi's sarcoma, primary effusion lymphoma, and multicentric Castleman's disease. *Am J Pathol*. 2000;156(3):743–749.

80. Nealon K, Newcomb WW, Pray TR, Craik CS, Brown JC, Kedes DH. Lytic replication of Kaposi's sarcoma-associated herpesvirus results in the formation of multiple capsid species: isolation and molecular characterization of A, B, and C capsids from a gammaherpesvirus. *J Virol*. 2001;75(6):2866–2878.

81. Lee GM, Thornthwaite JT, Rasch EM. Picogram per cell determination of DNA by flow cytofluorometry. *Anal Biochem*. 1984;137(1):221–226.

82. Garcia-Sepulveda CA, Carrillo-Acuna E, Guerra-Palomares SE, Barriga-Moreno M. Maxiprep genomic DNA extractions for molecular epidemiology studies and biorepositories. *Mol Biol Rep*. 2010;37(4):1883–1890.

83. Hayward IP, Parsons PG. Comparison of virus reactivation, DNA base damage, and cell cycle effects in autologous human melanoma cells resistant to methylating agents. *Cancer Res*. 1984;44(1):55–58.